Aufbau eines Motors mit zwei künstlichen Muskeln

Build up of a motor with two artificial muscles

Studienarbeit

Philipp Eiber

cand. ing.
Matrikelnummer: 2188616

Betreuer:

Prof. Marco Antonio Meggiolaro (PUC Rio)
Dipl.-Ing. Michael Seyfarth (Uni Stuttg.)

Pontifíca Universidade Católica do Rio de Janeiro
Universität Stuttgart

Institut für Steuerungstechnik der Werkzeugmaschinen
und Fertigungseinrichtungen

Januar 2010

_____

Eidesstattliche Erklärung

Hiermit erkläre ich, dass ich die vorliegende Arbeit selbstständig ohne fremde Hilfe bzw. unerlaubte Hilfsmittel angefertigt, andere als die angegebenen Quellen und Hilfsmittel nicht benutzt und die den benutzten Quellen wörtlich oder inhaltlich entnommenen Stellen als solche kenntlich gemacht habe.

Stuttgart, den 10. Januar 2010

_____

Philipp Eiber

_____

_____

Acknowledgement

This project was performed during a six month stay at Pontifíca Universidade Católica in Rio de Janeiro, Brazil.

The stay was supported by the Landesstifung Baden Würrtemberg. Prof. Hans Weber, from Departmento Mechânica, iniciated the project and the word was done in the Laboratório dos Rôbos under the guidance of Prof. Marco Antonio Meggilario. I was friendly integrated in the team and there was prosporous interaction between the students. At the University of Stuttgart the work was supervised by Dipl. Ing. Michael Seyfarth, Institut für Steuerungstechnik der Werkzeugmaschinen und Fertigungsanrichtungen.

My sincere Thanks goes to all institutions and persons whos made this project possible.

_____

Inhaltsverzeichnis

List of Figures

List of Pictures

List of Tables

1 Introduction

The development of technical machines and devices especially in the "Bionic" field are often closely oriented on principles known from nature.

In this work an artificial muscle in considered and its behaviour in particular high frequencies is analyzed. A motor with two artificial muscles was built which is used for research purpose and for teaching students in mechatronics.

Chapter 2 introduces some basic information about mammal muscles, conventional actuators and artificial muscles. Furthermore, it shows application areas for artificial muscles and compares them to conventional actuators. Chapter 3 introduces the motor with detailed information about each component. Finally, a mathematic model of the motor was derived. The following chapter analyzes several experiments with the motor under different conditions. In chapter 5 the results of the simulation, based on the mathematic model, are shown and compared to the results of the measurements in chapter 4. At the end, a conclusion of this work is given.

2 Actuators

2.1 Introduction to mammals muscles

In this chapter the mammal muscles are introduced to compare it with the artificial muscle. This should only show the functionality of the muscle and is far away from a detailed description.

Mammals have two different types of muscles: smooth and striated, whereas the striated muscles can be distinguished between cardiac and skeletal muscles. Smooth muscles are not under conscious control and exist e.g. in intestines or blood vessels. The cardiac muscle is the actuator of the heart. Skeletal muscles are usually connected to the bones with tendons and can contract voluntarily or involuntarily due to reflexes. The force generated by the muscles is transmitted by the tendons to the bones where they may generate a torque in the belonging joint.

For the humanoid robots, skeletal muscles are of interest because they are responsible for the movement.

Figure 2-1 shows the composition and dimension of a skeletal muscle in detail.
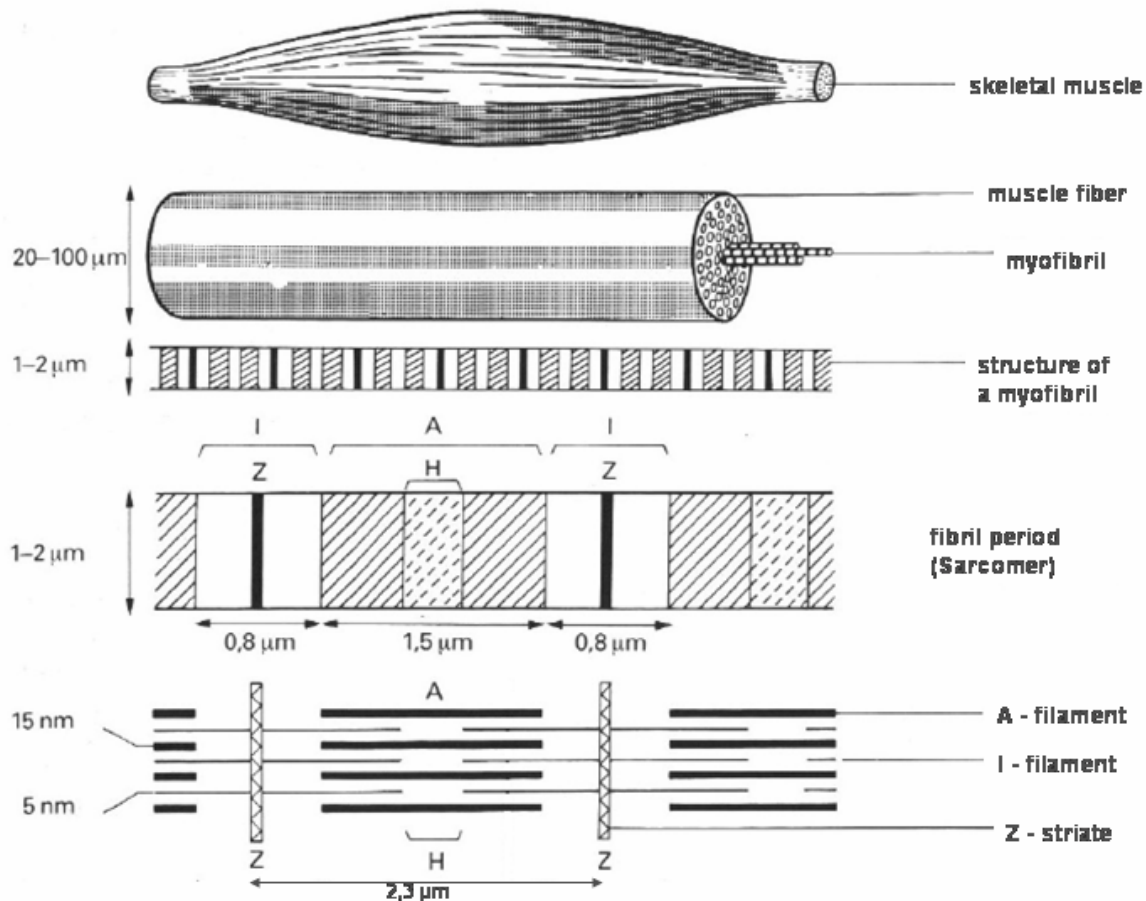
Figure 2-1 Striated muscles [1]

Each striated muscle has various bundles of fibers. An adult human has an average muscle fiber diameter of 50µm whereas a frog has about 100µm. Nerve fibers, blood and lymphatic vessels are throughout the whole muscle.

These fibers again are bundles of smaller fibers, called Myofibril. They have typically a diameter of 2µm. The fibers are split up in a series of smaller units, called Sarcomeres. The discs between the Sarcomeres give the muscle their typically look. The Sarcomeres are responsible for the contraction.

Around the Myofibril is a membrane called sarcoplasmic reticulum. This membrane accumulates ionics which are necessary for the contraction. By an electric impulse of the central nervous system, the membrane releases the ionics into the Myofibrils where they trigger a series of chemical reactions. These reactions cause the contraction in a Sarcomere. The Sarcomere has two different states of activation: released or contracted. The muscle force is controlled by the number of activated Sarcomeres and the direction of the force is like the orientation of the Sarcomeres.

While contracting, the white I-stripes are moving into the red A-stripes.

The generation of force can be categorized in isometric and isotonic contraction.

Isometric contraction is defined by a change of force without a change in muscle length. In this case, the maximal force depends on the actual length.

Whereas the isotonic contraction is defined by a constant force during contracting. The maximal force is depending on actual length and the actual velocity.

Skeletal muscles contain two main types of fibers:

- Slow-twitch or Red fibers.
- Fast-twitch or White fibers

White fibers are capable to move with high velocities and can produce high peak power but show a low endurance, whereas Red fibers are contrary to that features. For example a marathon runner has more Red fibers than a bodybuilder or sprinter, who has more White fibers.

In Figure 2-2 different shapes of skeletal muscles with its tendon appendages are shown.

a : simple spindle shaped muscle

b : two headed muscle (biceps)

c : three part muscle (deltoid)

d : spread muscle (anterior serratus muscle)

e : one side feathered muscle
(peroneus longus muscle)

f : double side feathered muscle
(tibialis anterior syndrome)

g : muscle with tendons (abdominal muscle)

h : biventral muscle (omohyoid muscle)

i : more tail muscle
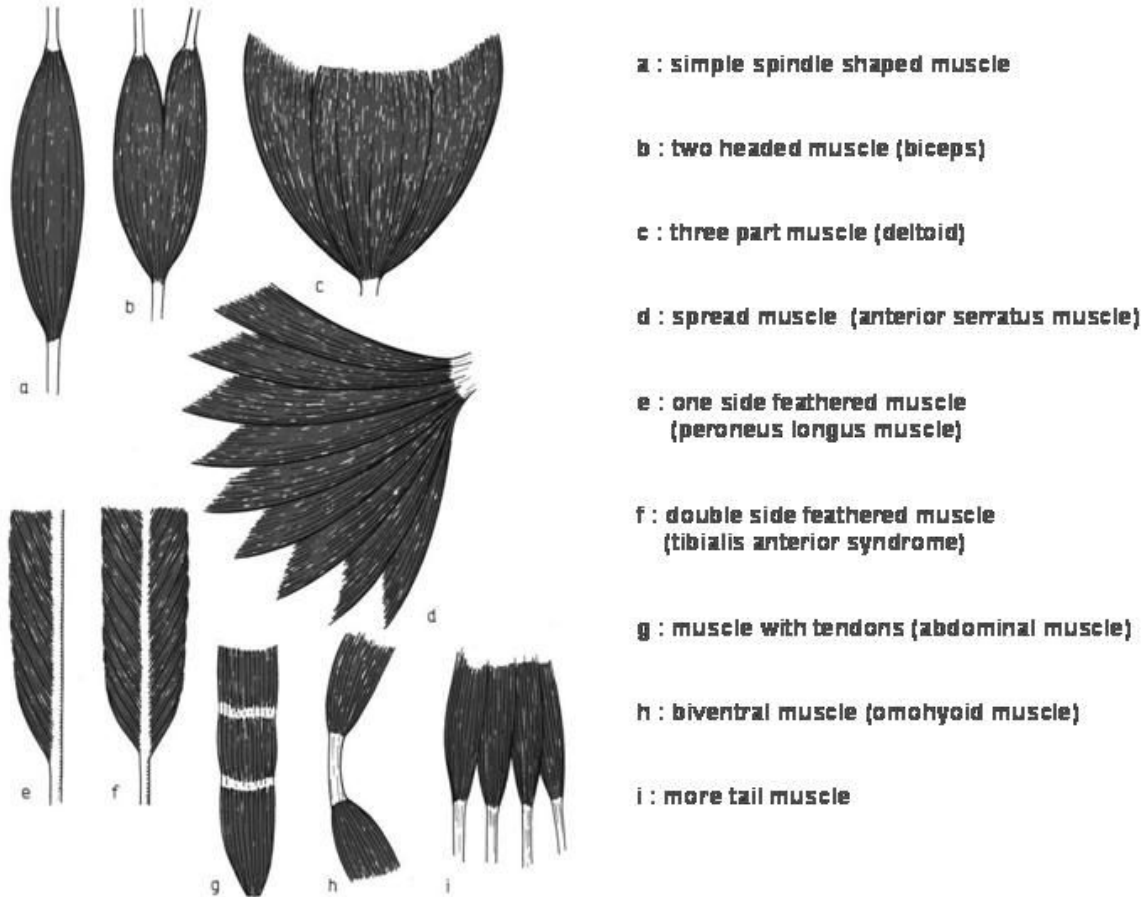
Figure 2-2 Striated muscles forms [1]

Parallel fibered muscles are quick actuators unlike feathered muscles which are strong force motors with a large cross-section.

2.2 Artificial actuators

This chapter introduces pneumatic actuators and compares them to hydraulic and electric actuators. Chapter 2.2.2 shows the Pneumatic Artificial Muscles (PAM) and points out their advantages and disadvantages. In chapter 2.2.3 application examples are given.

2.2.1 Pneumatic actuators

Pneumatic systems have a long history. The first written document is the "Temple doors of Alexandria" from 60 A.D. Meanwhile pneumatics plays an important role in the industry, especially in the automation section. Pneumatics can be found in different applications like pneumatic tools, drives and control systems. A pneumatic system consists of three subsystems:

- generation of pressurized-air
- compressed-air conditioning and allocation
- control system and actuation elements

Some advantages and disadvantage of the pneumatic, hydraulic and electric systems and actuators are shown in Table 2-1.

Table 2-1 Characteristics of different actuator principles

	Advantages	Disadvantages
Pneumatic	- air is widely available - non polluting medium - high speeds reachable - overloading possible - no return line required - works in explosive areas - light weight	- air compressible (control of motion difficult) - noise pollution - bad efficiency - temperature dependence of the medium (air conditioning necessary)
Hydraulic	- high power to weight ratio - self lubricating and cooling - speed precisely controllable - generating of high forces - high lifetime - good servo control - fast response - smooth operation in low speed	- expensive - high requirements needed for filtering the medium - high requirements needed to prevent leaks - return line required - temperature dependence of the medium

Electric	• fast and accurate • control techniques simply to apply • widespread • cost efficient • quiet	• problems to use in explosive areas • problems with overheating • breaks are needed to lock motors • low power to weight ratio

For the selection of driving principle, the specific problem at hand defines which system is the best.

2.2.2   Pneumatic Artificial Muscle PAM

Last chapter showed the conventional actuators with their advantages and disadvantages. In the field of robotic, especially for running and jumping machines or humanoid robots, actuators similar to natural muscles are necessary. The specific requirements concern lightweight, direct drive and passive damping.

Different kinds of artificial muscles are:

- Pneumatic artificial muscles (PAM) / Fluidic Muscle

- Chemical muscles (SMP, LAP)

- Electroactiv polymer (EAP)

- Piezoelectric actuators

The functionality of the PAMs is very simple and follows the McKibben concept. It is a flexible rubber tube with an embedded weave and attached with two connectors at each side. As the muscle is inflated with pressurized air, the tube expands in radial direction and because of the non stretchable weave the muscle contracts in axial direction. The weave can be seen in Figure 2-3. The right side illustrates the actuator in relaxed and contracted condition.
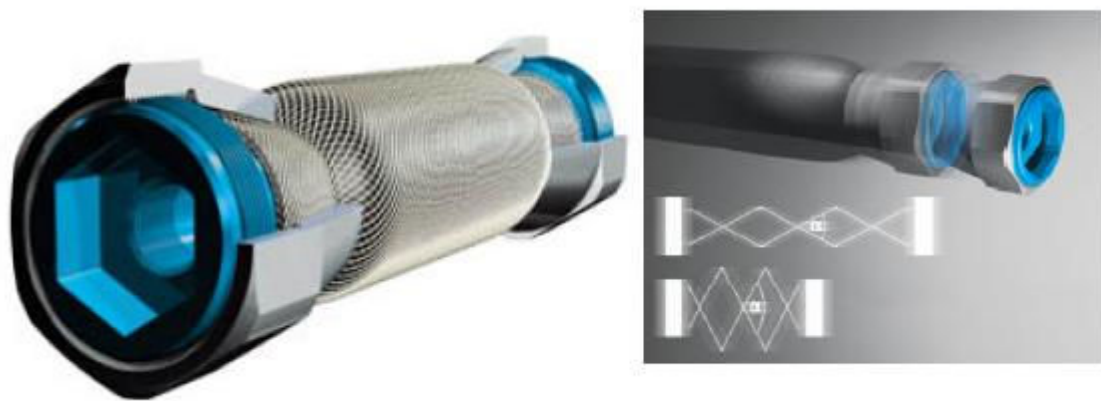
Figure 2-3 Festo's PAM

Without an external load, the muscle can reach a stroke up to 25%. The external tensile force depends on the actual length and the pressure inside the tube. At the contraction of zero, the muscle has its biggest force, which decreases nonlinearly by the contraction stroke.

Festo offers two types of PAM, conventional one is called MAS and a light weight type called DMSP. Both types are available in different diameters and connector versions: with a force limiter (-K) and without force limiter. An example of Festo's nomenclature is given in Figure 3-2. In this project MAS-10 without force limiter is used. Figure 2-4 shows the operating range of the MAS-10.
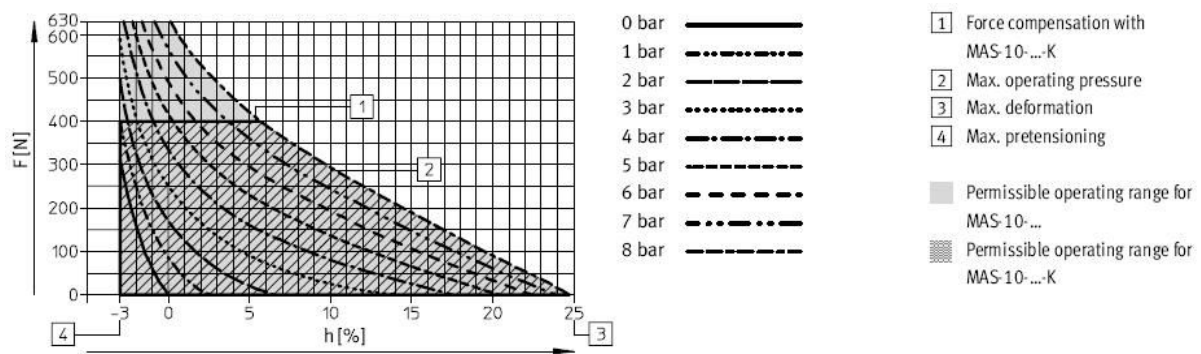
Figure 2-4 Operating range of Festo's PAM for a diameter of 10mm

Line 1 shows the force limit of the MAS-10 -K. The type DMSP has 30% less weight than the MAS and therefore a better power to weight ratio.

PAM´s have several advantages which makes these actuators very interesting for humanoid robotics.

The advantages of the PAM are:

- no stick-slip effect

- no extra moving parts

- high power to weight ratio around 1000 W/kg

- high dynamic response

- simple construction

- high speed (3 m/s)

- high acceleration (100 m/s^2)

- passive damping

- hermetically sealed design

- can operate with gas or fluids

But PAM´s have also disadvantages which cannot be neglected:

- gas is compressible

- nonlinear force

- not able to push

- position control is difficult

- not autonomous because it requires pressurized air

An example of an fluid driven actuator is the artificial fish Aqua-ray, shown in chapter 2.2.3.

Like mammal muscles, artificial muscles are normally implemented in an antagonistic concept see in Figure 2-5 because they are only able to pull.
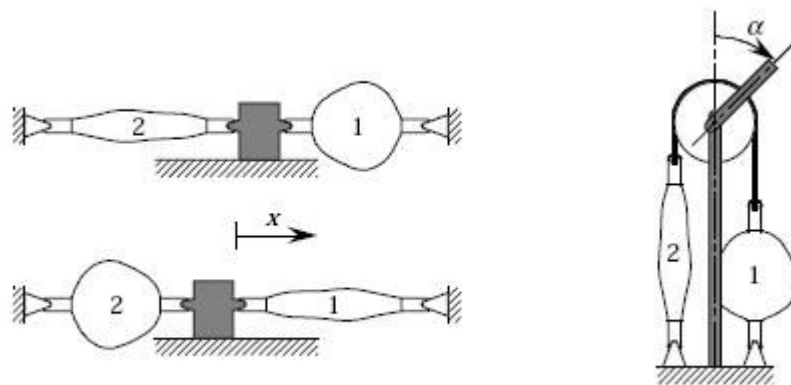
Figure 2-5 Antagonistic principle [5]

2.2.3   Application examples

A few examples of pure pulling are shown in Figure 2-6.
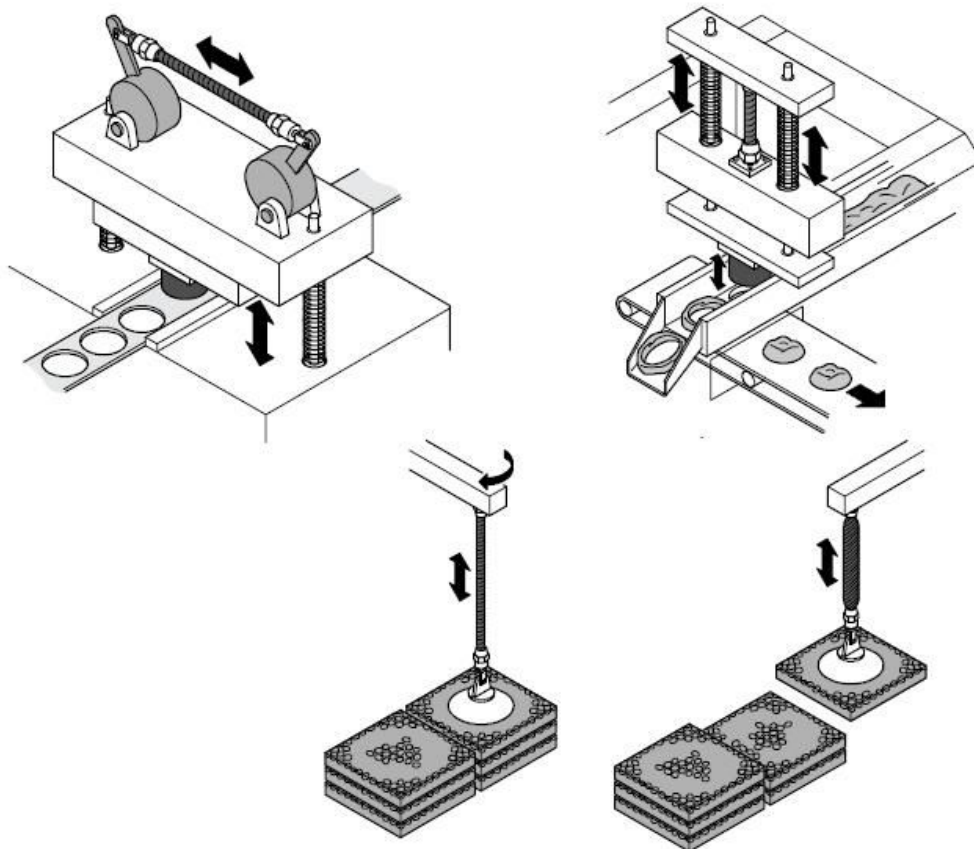
Figure 2-6 Simple applications [3]

Even more interesting application areas are offered in the robotics and bionic area. For the field of climbing, walking and running robots, the pneumatic muscle is a good alternative to the commonly used electric actuators. Several research groups are working on the implementation of PAMs into production robots, see e.g. [13], [14].

One interesting example of walking robots is the six legged insect like "AirBug" which was developed at the "Forschungszentrum Informatik" at the University of Karlsruhe. It is shown in Figure 2-7.

Figure 2-7 Air Bug [4]

In cooperation with universities and other companies, Festo promotes ideas and initiatives in the bionic field in their "Bionic Learning Network".

Using nature as a model, they presented several prototypes. In the following, three interesting projects from Festo are illustrated.

The "Airmotion Ride" is a driving and flight simulator based on a hexapod structure. Six spatially oriented MAS-20 are able to move the seat in all 6 axes. The solution as shown in Figure 2-8 with pneumatic muscles is a cost effective alternative to complicated hydraulic systems. The PAMs also serve as a passive suspension of the seat.

Figure 2-8 Airmotion Ride [3]

The second project, called "Airic´s arm" mimics a human arm. It is a robotic arm with artificial bones and muscles. The bone structure is moved via 30 muscles. With new and very small valves based on piezo technology, Festo was able to put the whole controle system close to the muscles. In the next step, sensors are going to be implemented to get a closer behaviour to the human arm.

Figure 2-9 shows the arm from the right side.

Figure 2-9 Airic´s Arm [3]

"Aqua ray" is a remotely controlled fish using water hydraulic driven Fluidic Muscles. The form and kinematics are modeled on the movement's patterns of the manta ray. Six muscles in three antagonistic pairs are moving the two wings and the tail with the help of artificial tendons. The fish is using the "Fin Ray Effect®", an almost perfect and very efficient imitation of a fish's fin. "Aqua ray" can either glide or flap actively with its wings to move forward.

The artificial fish is illustrated in Figure 2-10.
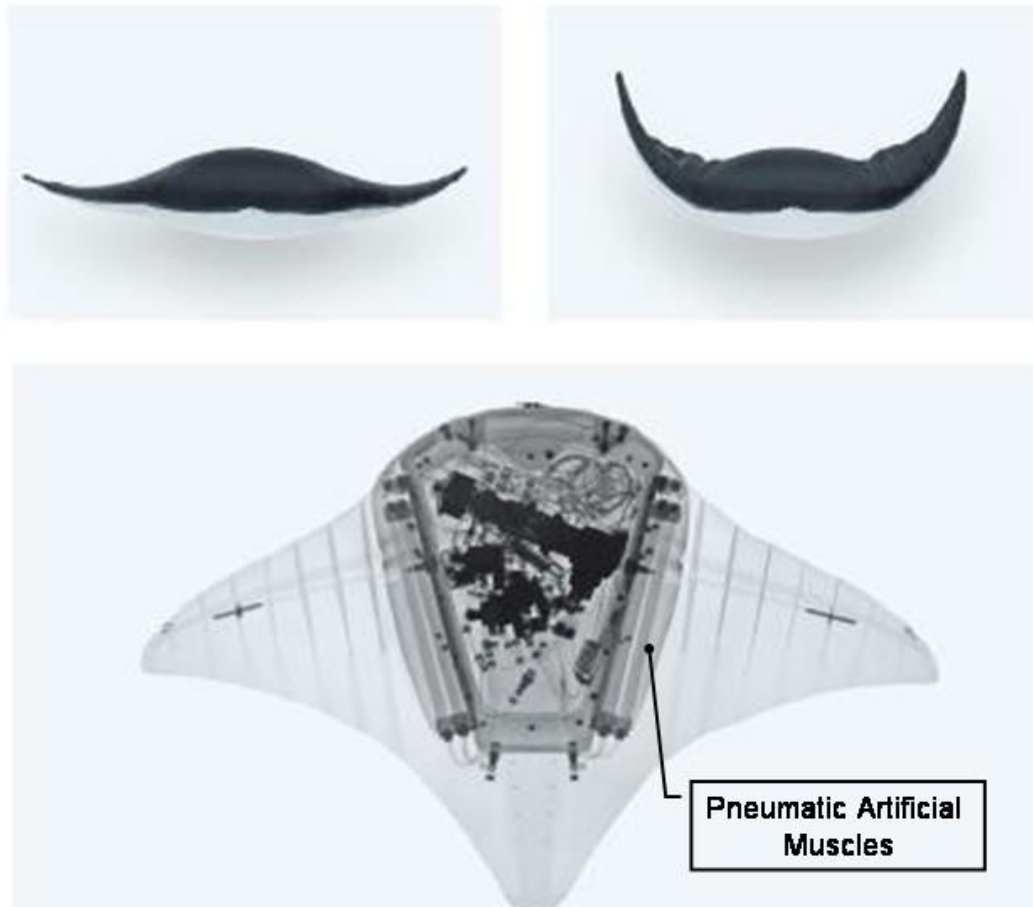
Figure 2-10 Artificial fish Aqua Ray [3]

2.3 Mammal Muscles compared to Fluidic Muscles

A direct comparison of the variables between the mammal's skeletal muscle and the MAS is difficult because there are a lot different kinds of mammal's muscles. Only two ended muscles like the biceps are comparable.

Some mechanical properties are summarized in Table 2-2. I turns out, that skeletal muscles are better in strain, contracting range and life cycles. They also have a better versatility than artificial muscles. An advantage of the fluidic muscle is a good power to weight ratio.

Table 2-2 Comparison of biological vs. fluidic muscle [2]

	biological muscle	pneumatic artifical muscle
contraction	50 - 70 %	max. 35 %
force / cm²	20 - 60 N	up to 700 N
power / kg	40 - 250 W/kg	0.5-2 kW/kg
efficiency	20 - 30 %	22 - 50 %
speed of contraction	up to 8 m/s	up to 2 m/s
frequency	20 - 100 Hz convulsions	5 Hz
controllability	good to excellent	satisfactory to good
operation in water	yes	yes
temperature	0-40 °C	-30 - 80 °C
regeneration	yes	no
energy source	chemical	pneumatic
environment	produce CO_2	depends on pressure editing
scalable in	µm - m	mm - m
linear drive	yes	yes

An amazing feature is that a mammal muscle can grow and modify itself. It also can repair itself. The human proteins in human muscles are renewed every few months. So far, these features are not achieved in any known technology.

3 Motor

Chapter 3.1 introduces the units of the motor. The following chapter shows the design and functionality of the motor units. In chapter 3.3 the mathematic model of the fluidic muscle and the motor is derived.

3.1 Function of the Motor

This motor is a good device to analyze the muscle and its behaviour especially on high frequencies. Furthermore, it was built as an educational set up for the mechatronic students.

Picture 3-1 shows the different components of the motor:
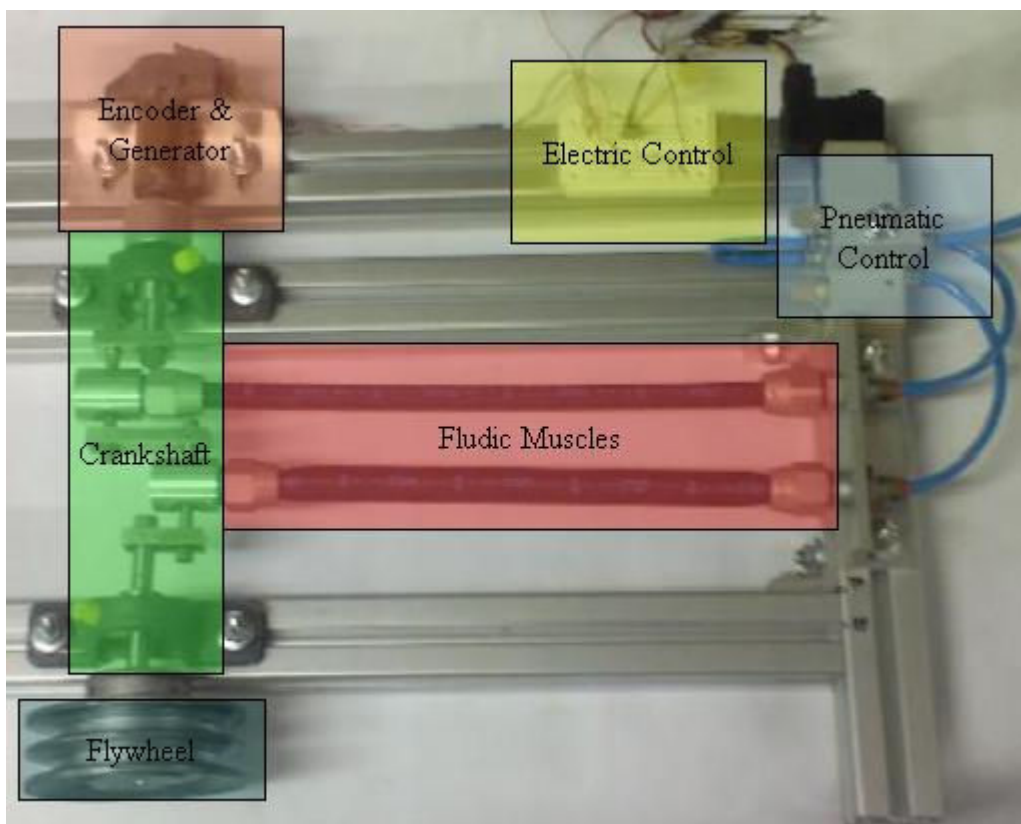
Picture 3-1 Motor units

The units are:

- Fludic Muscles as actuators

- Pneumatic and Electric Control unit is controlling the muscles

- Encoder & Generator unit first measures the state of the shaft over an optocoupler (Enconder). A DC motor, available in the lab, is used as a tacho generator. The generated voltage is proportional to the rotation speed

- Crank shaft to convert the linear actuation into a rotation

A detailed explanation of each unit is given in the following chapter.

The principle of the motor is simple. Two alternately contracting actuators affect a force on the crank shaft, similar to a two cylinder combustion engine. The half-disc is setting the optocoupler status which controls the directional valve. Thus, there two cycles per revolution defined. The two cycles can be shifted with suspect to crank shaft angle, see in chapter 4.2. Without a shift angle the following function diagram is valid.
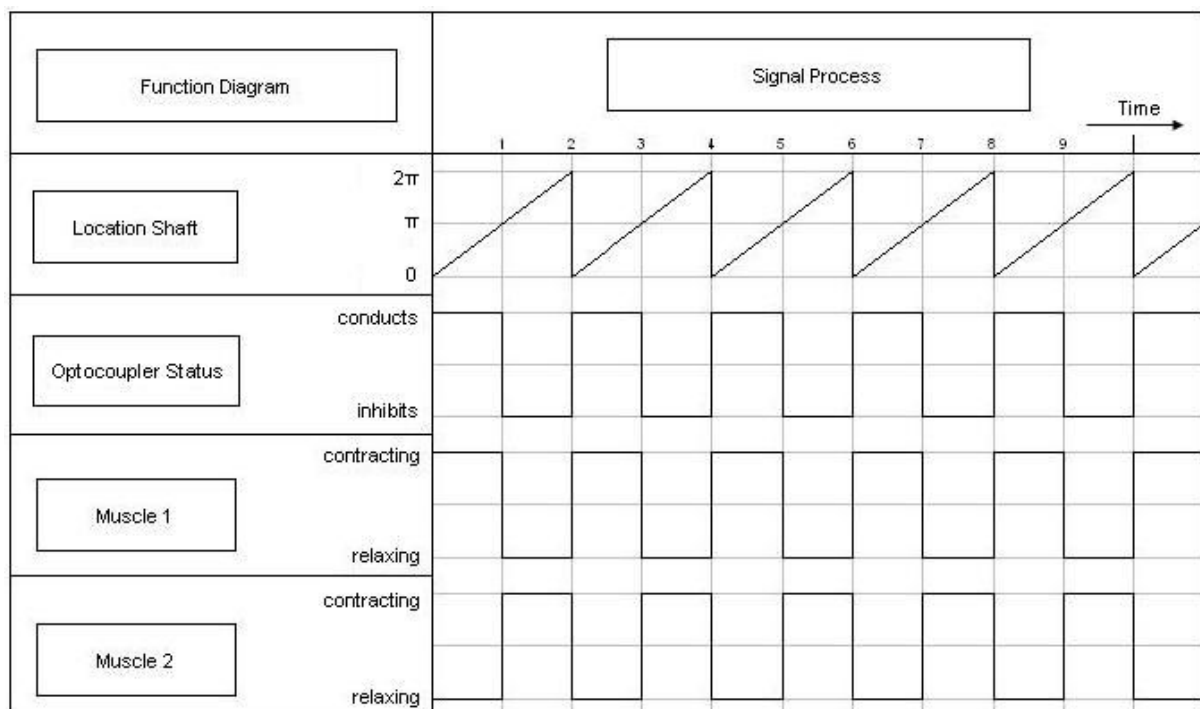
Figure 3-1 Function Diagram of the motor

3.2 Motor design

Because of their flexible use and the easy adjustment of the units the frame was built with standard aluminium profiles. The size of the frame allows the use of bigger muscles.

3.2.1 Muscle unit

The basic description is already is given in chapter 2.2.2. This chapter shows the mechanical properties of the used actuators. For these muscles Festo's nomenclature is illustrated in Figure 3-2.

Used Muscles: MAS-10-300N-AA-MC-O

Fluidic Muscle type
Nominal diameter in mm
Nominal length in mm
Standard material (Cloroprene, Aramid)
One supply connector (2 connectors: -M0)
Without Force limiter (with limiter: -K)
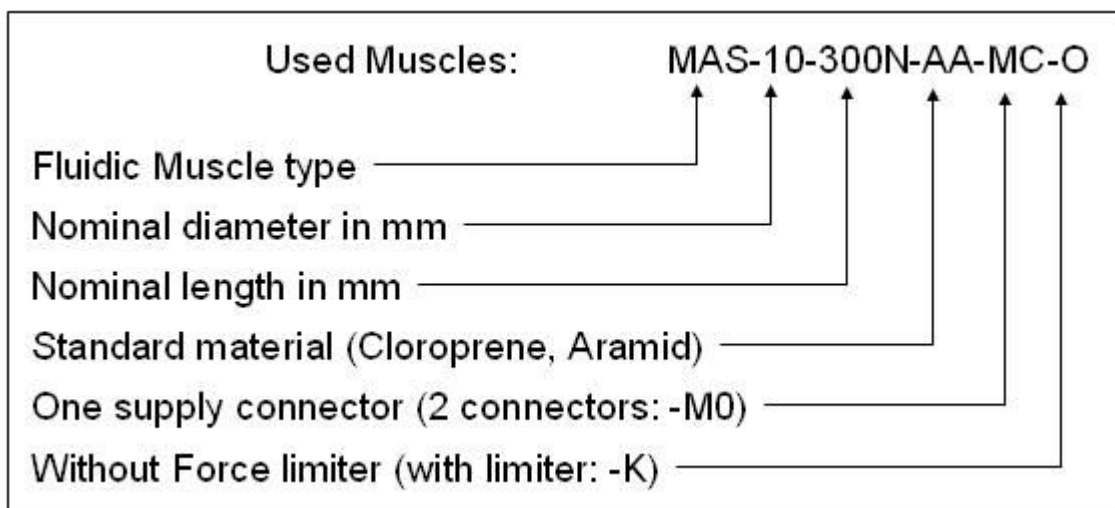
Figure 3-2 Festo's Nomenclature

The muscles are working in a range between 0 and 8 bar relative pressure and are contracting between 0% and 15%. The generated force is between 630N at 0% contraction and 200N at 15% contraction. This working area is marked in red, Figure 3-3.
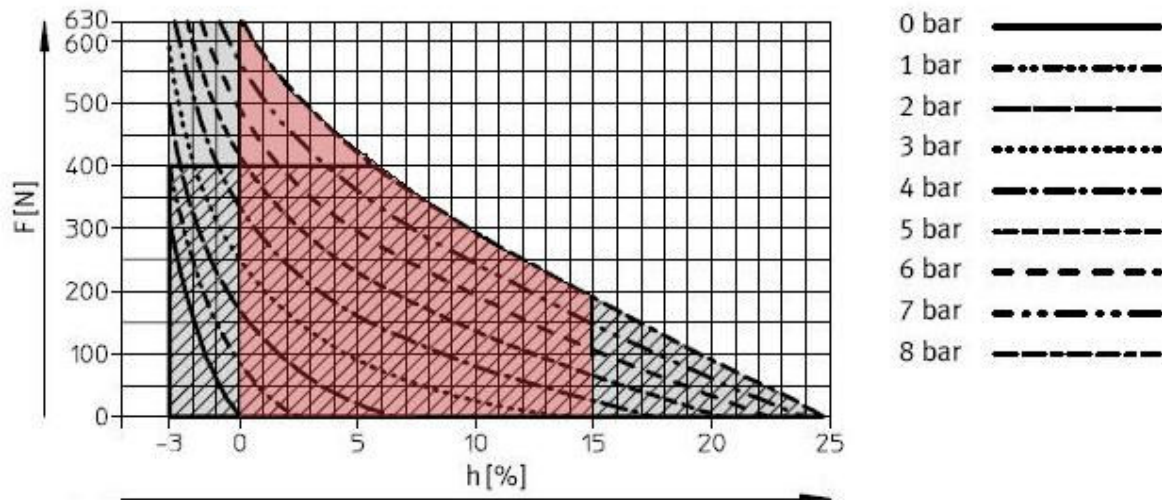
Figure 3-3 Operating Range

3.2.2 Shaft unit

For the design of the motor some properties are required: The motor has to be demountable in order to attach the actuator over a connector at the crank of the shaft. The use of roller bearings does not allow a crank shaft as a single piece.

The second important required property is a high bending stiffness. In the static worst case a force of 630N affects on the shaft.

Most important for a smooth rotation are adequate and accurate manufactured parts. Static or dynamic unbalances as well as geometrical imperfect assembling of the parts cause undesired vibrations.

The final construction is shown Picture 3-2.
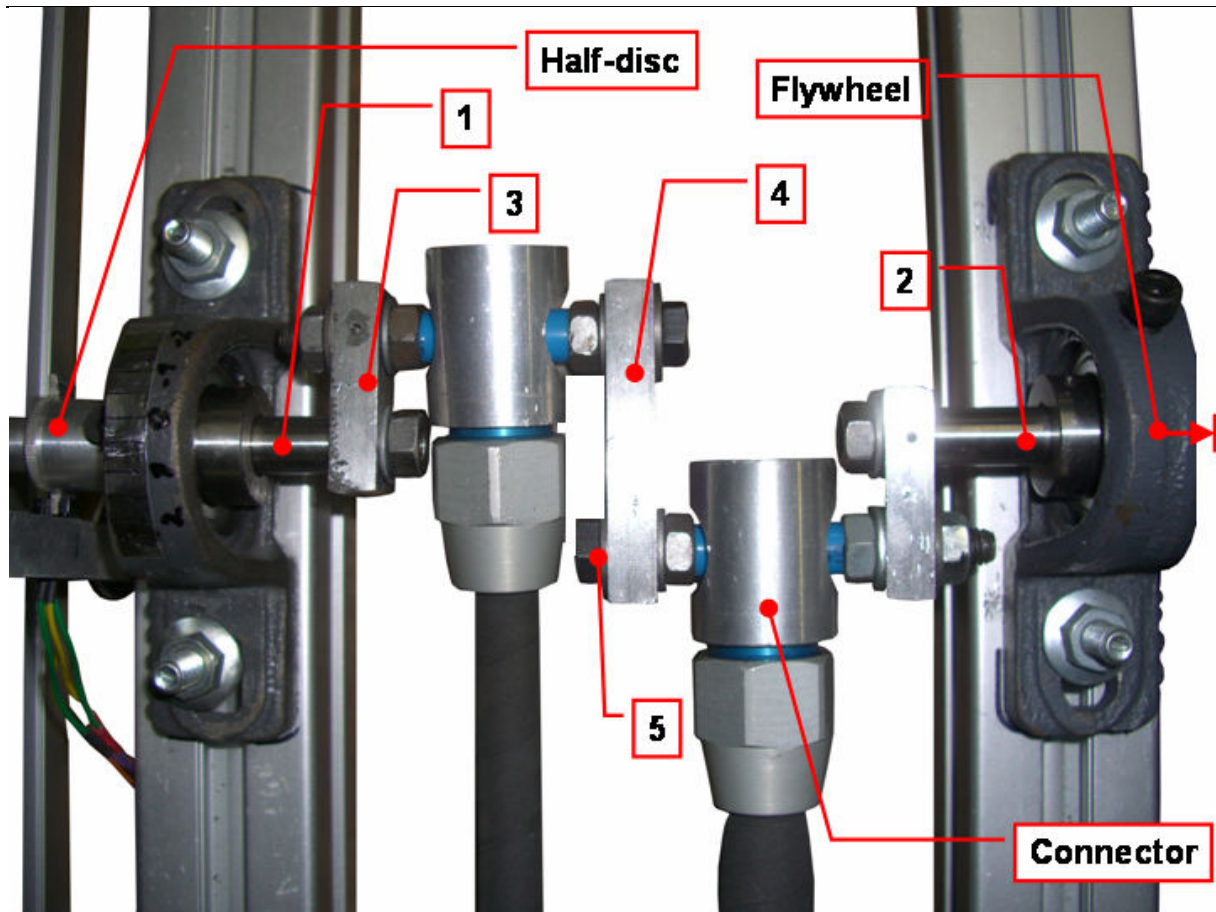
Picture 3-2 Shaft Construction and label

The shaft is made up of seven parts. Number 1 and 2 are round shafts. Number 3 are identical arms and 4 is the middle arm. For simplicity, the two cranks number 5 are realized by two M8x100 12.3 screws. The parts are connected with threads and part 1 and 2 have additionally split pins. The shaft has a weight of m = 0.538kg and a moment of inertia of $J = 2.347 \text{kg cm}^2$.

The shaft is supported by two pedestal bearings to the frame. One side is fixed by a set screw the other side has an axially loose connection.

In the connectors are roller bearings which are positioned by spacers (blue) on the cranks.

On the left side there is an adjustable connector to the electric DC motor which is used as a tacho generator. The adjustment is shown in Figure 4-6. The connector carries also the half-disc which is used for the control of the directional valve.

3.2.3 Flywheel mass

The motor has two singularity points which are at 0π/2π and π. Because of not exactly assembled elements and mounting tolerances, these points are slightly shifted. This leads to an asymmetric behaviour (two different cycles) during a revolution. It also could cause the motor to oscillate rather than to rotate. To prevent an oscillating behaviour an, a flywheel is attached to turn the shaft over the singularity points.

The flywheel is a steel disc with a mass of 3.2 kg and a moment of inertia of J = 52.903 kg cm^2

3.2.4 Encoder & Generator unit

3.2.4.1 Encoder

The encoder's task is to detect the position state of the crankshaft and to provide this information to the control system. Commonly, resolvers with resolutions up to 4000 steps in one turn are used for position control.

In this project, the encoder is simply realized by an optocoupler and a half-disc delivering only two states per turn. The optocoupler is shown in Figure 3-4.
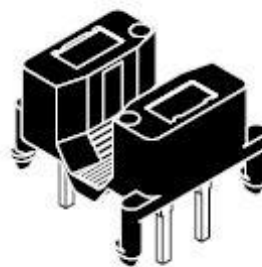
Figure 3-4 Optocoupler

The sensor consists of a light emitting diode and a photo transistor. If there is a non light-transmissive material between the sensors, then the optocoupler inhibits

otherwise it conducts. Chapter 3.2.5 explains the circuit diagram with the optocoupler.

3.2.4.2 Generator

The generator is used to measure the rotation speed. It is a brushless DC motor with a permanent magnet. These kinds of electric motors have a proportional relation between speed and voltage. For the used electric generator it holds

$$n = k_n \cdot U \quad , \quad k_n = 713 \, \frac{rpm}{V}$$

where the rotation speed is n, k_n the proportional constant and U the measured voltage.

To interpret this analog signal, it is converted into a digital signal via the A/D converter USB 6009 from National Instruments.

3.2.5   Electric unit

The electric unit needs two power supplies with different voltages, V1 with 5 Volts for the optocoupler and V2 with 24 Volts, for the inductor. The inductor L1 triggers the pneumatic directional valve.

During an inhibiting optocoupler no current flows at the base of Q1, so it inhibits too. When the optocoupler conducts, Q1 also conducts and therefore the inductor L1 triggers the valve until the optocouplers inhibits again.

The diode D1 implemented parallel to L1 is protecting Q1 of an inverted voltage push. This happens when Q1 changes the state from conducting to inhibiting, due to the inductance of L1. The circuit and the notations are shown in Figure 3-5:
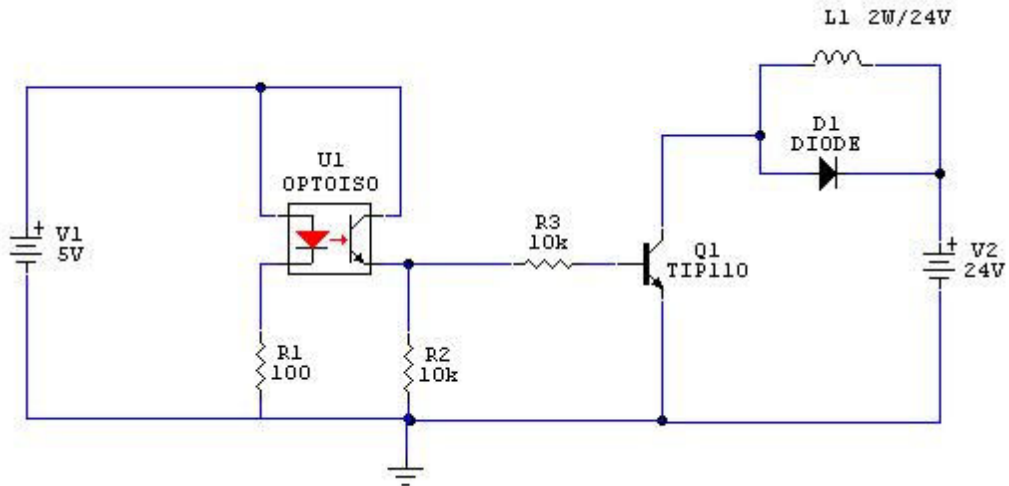
Figure 3-5 Electric circuit diagram

3.2.6   Pneumatic unit

Two parts are controlling the pneumatic part of the motor:
- a mechanically adjustable flow-control valve (throttle)
- a 24 Volts monostable 5/2 directional valve

The flow-control valve is adjusted manually via a spindle, which has a range of 14 turns from fully open (100%) to completely close (0%). The opening of the valve is indicated by the percentage.

Figure 3-6 shows the pneumatic circuit diagram
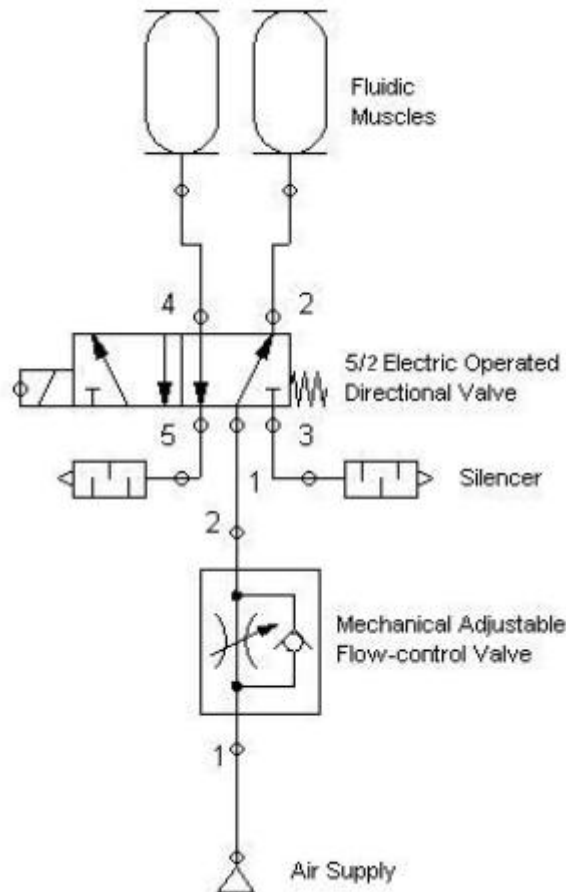
Figure 3-6 Pneumatic circuit diagram

In this condition, sketched in Figure 3-6, the right muscle is contracting. The contracting speed is limited by the air flow which passes the flow-control valve. Consequently the maximum speed is limited. The outgoing air of the left muscle is limited by the flow resistance. One significant fact is the small diameters in the muscle connectors and the silencers.

3.2.7 Block Diagram

The block diagram shows the interaction between these units. The massflow from the supply is routed by the pneumatic block to the actuators. The contracting actuator generates a force which affects a momentum in the shaft. Output is a rotation of the shaft. In the electric bloc the optocoupler measures the state of the shaft for triggering the pneumatic valve.
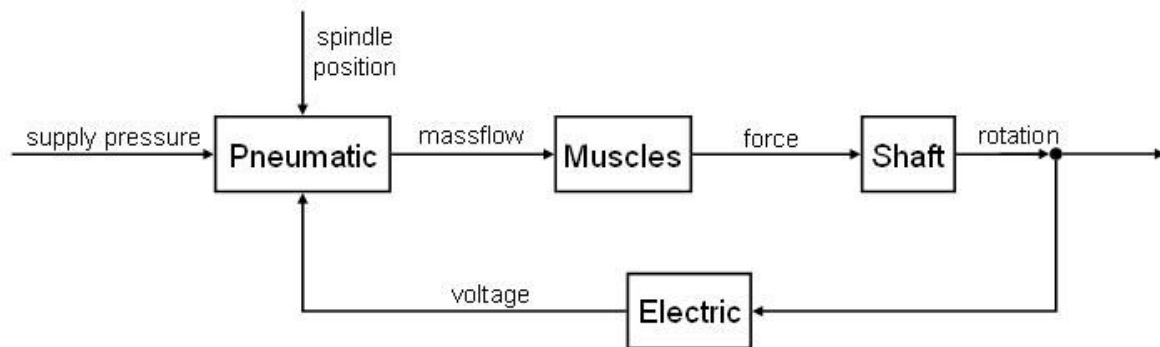
Figure 3-7 Block diagram

3.3 Mathematic Model

In this chapter mathematic equations are derived to simulate the dynamic behavior of the motor. The modeling process is based on Matlab/Simulink.

3.3.1 Force of the muscle

Sub-chapter 3.3.1.1 shows the mathematic background of the muscle simulation program "MuscleSim" from Festo. This program was used as an alternative to measurements of the force, which was not possible because of the non-availability of measurement equipment. The derivation of the force equation based on the simulation data from Festo shows sub-chapter 3.3.1.2

3.3.1.1 Background "MuscleSim" Program from Festo

The fluidic muscle from Festo follows the McKibben principle which was invented in the 1950s by physician Joseph L. McKibben. This model for the muscle generally depends on the pressure and the three muscle parameters:

- initial weave angle (angle between fibres and length axis)
- initial length of the muscle
- initial radius

The derivation of this model is well described by Tondu and Lopez in [10] and Chou and Hannaford in [11].

Festo uses another approach to describe the force of the muscle mathematically. The model as described in [12] is an approximation to a pneumatic cylinder with a mechanical return spring, shown in Figure 3-8.
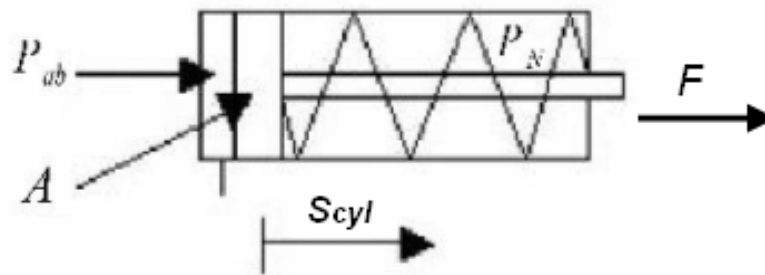
Figure 3-8 Pneumatic cylinder with mechanical return spring

In this case the force depends on the:

- piston's surface A
- absolute pressure P_{ab}
- ambient pressure P_N
- spring characteristic c
- displacement $s_{cyl.}$

To describe the nonlinear, degressive muscle behaviour as shown in shown in Figure 2-4, the spring characteristic must be nonlinear. In Festo [12] the force is given as

$$F(s, P) = P \cdot A_v - \left(c_1 + c_{1p} \cdot P_{ab}\right) \cdot s - c_2 \cdot s^2 - c_3 \cdot s^3,$$

Equation 3.1

where $P = P_{ab} - P_N$. And A_v is representing a virtual surface which is derived by a differentiation of a volume equation. The stroke $s = l_0 - l$ is defined as the initial length minus the actual length. For a muscle with a diameter of 10mm the virtual surface is 33mm. This means that at stroke of zero the muscle has an 11 times higher force than a pneumatic cylinder with the same diameter.

The Equation 3.1 is used in the program "MuscleSim". For given diameter and length of the muscle, pressure and actual stroke the program calculaters force of the muscle as shown in Table 3-1.

Table 3-1 "MuscleSim" results of the force depending on pressure and stroke

rel. pressure [bar] \ stroke [mm]	0	5	10	15	20	25	30	35	40	45	50	55	60	65	70	75
0	0	0	0	0	0	0	0	0	0	0	0	0	0	0	0	0
0,5	41,4	0	0	0	0	0	0	0	0	0	0	0	0	0	0	0
1	82,6	18,1	0	0	0	0	0	0	0	0	0	0	0	0	0	0
1,5	123,4	57,2	14,9	0	0	0	0	0	0	0	0	0	0	0	0	0
2	164	96,1	51,8	21,3	0	0	0	0	0	0	0	0	0	0	0	0
2,5	204,2	134,6	88,4	55,8	31,7	13	0	0	0	0	0	0	0	0	0	0
3	244,1	172,9	124,8	90,2	63,7	42,6	25,1	10,1	0	0	0	0	0	0	0	0
3,5	283,8	210,8	161	124,3	95,7	72,2	52,3	34,7	19	4,5	0	0	0	0	0	0
4	323	248,5	196,9	158,3	127,6	101,8	79,5	59,2	41,2	24,3	8,3	0	0	0	0	0
4,5	362	285,5	232,5	192,1	159,3	131,4	106,8	84,4	63,7	44,3	25,8	8,1	0	0	0	0
5	400,6	322,8	267,9	225,7	191	161	134,1	109,5	86,4	64,6	43,7	23,6	4,2	0	0	0
5,5	438,9	359,5	303	259,1	222,5	190,4	161,5	134,6	109,3	85,2	62	39,5	17,7	0	0	0
6	476,8	395,8	337,8	292,2	253,8	219,9	188,9	159,9	132,4	106,1	86,6	55,9	31,8	8,2	0	0
6,5	514,3	431,8	372,4	325,2	285,1	249,3	216,3	185,3	155,7	132,8	99,5	72,6	46,3	25,5	0	0
7	551,5	467,5	406,6	357,9	316,1	278,6	243,7	210,8	179,1	148,6	118,8	89,8	61,3	33,4	5,9	0
7,5	588,3	502,8	440,5	390,4	347,1	307,8	271,2	236,3	202,8	170,2	138,4	107,3	76,8	46,8	17,2	0
8	624,7	537,7	474,2	422,7	377,8	337	298,6	262	226,6	192,1	158,4	125,3	92,8	60,8	29,2	0

The GUI of the "MuscleSim" program is illustrated in Figure 2-1.

Figure 3-9 GUI of "MuscleSim", Festo

3.3.1.2 Derivation of the force equation

Because of problems to indicate the weave angle by the McKibben principle and to get the coefficients of Festo's equation, an own equation of the force was derived. It is similar to Festo's equation and depends on the pressure and stroke. The stroke s is defined as the initial length of the muscle minus the actual length.

$$F(s, P) = (c_{12} + c_{11} \cdot P) \cdot s^3 + (c_{22} + c_{21} \cdot P) \cdot s^2 + (c_{32} + c_{31} \cdot P) \cdot s + c_4 \cdot P$$

Equation 3.2

The coefficients were determined with the polyfit method in Matlab based on data from the muscle simulation program "MuscleSim" from Festo because the forces could not be measured in this project.
In Figure 3-10 the fit of the model and MuscleSim is figured out.
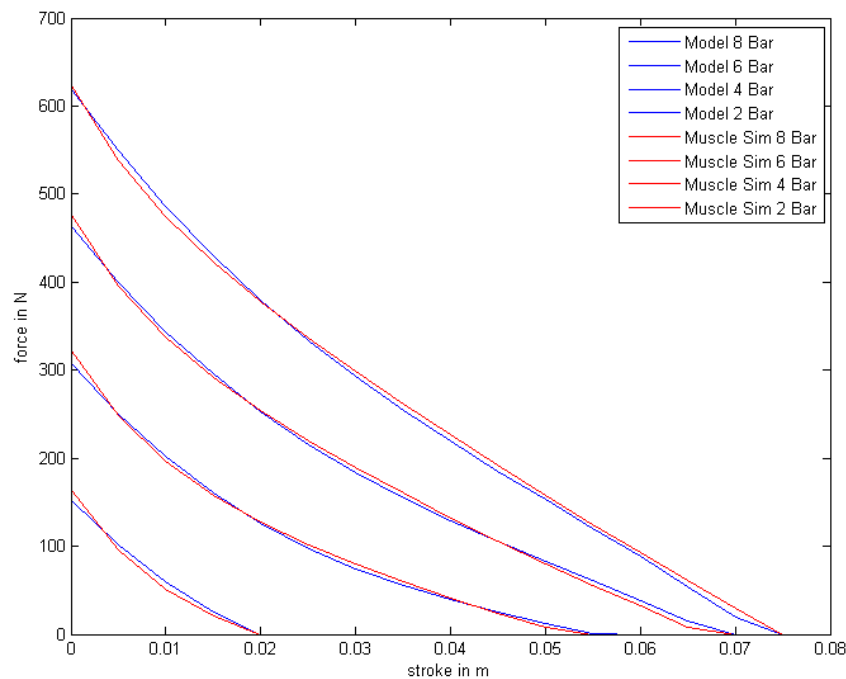
Figure 3-10 Fit of the model

The red curves are representing the values of the "MuscleSim" program of Table 3-1. The blue curves are the results of Equation 3.2.

3.3.2 Volume behaviour of the muscle

The equation of the volume is also similar to the equation of Festo [12]. The volume of the muscle depends only on the state of contraction and the initial length. The equation is a polynomial of third degree:

$$V(s) = v_1 \cdot l^3 + v_2 \cdot l^2 + v_3 \cdot l + v_4 \quad ,$$

Equation 3.3

,

where $l = l_0 - s$.

The coefficients were also found from the data of the MuscleSim. Figure 3-11 shows the volume depending on the stroke.
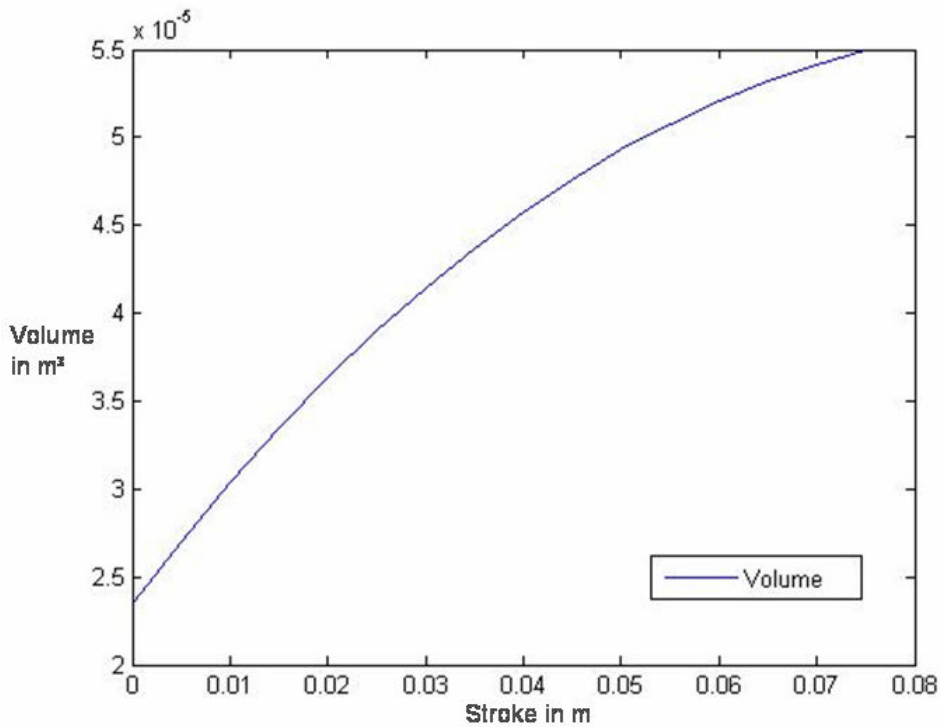
Figure 3-11 Volume vs. stroke for a MAS-10 with 300mm initial length

The values of the "MuscleSim" program are in Table 3-2:

Table 3-2 "MuscleSim" results of the volume depending on the stroke

Length in m	0,3	0,295	0,29	0,285	0,28	0,275	0,27	0,265	0,26	0,255	0,25	0,245	0,24	0,235	0,23	0,225
Vol in m³	2,36	2,66	3,06	3,36	3,66	3,86	4,16	4,36	4,56	4,76	4,96	5,06	5,16	5,36	5,46	5,46

The volume cannot be zero, because the muscle has a diameter of 10 mm in the initial state.

3.3.3 Pressure

The current state of the air inside the muscle can be described with the help of the model of ideal gas, [9] which is used in this mathematic model.

$$p \cdot V = m \cdot R_s \cdot T$$

Equation 3.4

- p is the pressure

- V describes the volume

- m is the mass of the considered gas volumen

- R_s he specific gas constant which is $288\dfrac{J}{kg \cdot K}$

- T is the gas temperature

This simplification is sufficient for most of the thermodynamic process in the technical area.

Any real variation of pressure and volume inside the muscle is between the ideal conditions of isothermal and adiabatic. This process can be described by the polytrophic gas law.

$$p_1 \cdot V_1{}^{\chi} = p_2 \cdot V_2{}^{\chi} = const$$

Equation 3.5

where χ is the polytrophic exponent. For $\chi = 1$ it describes a full isothermal process and for $\chi = 1.4$ an absolute adiabatic process.

The exact value is determined experimentally for each actuator or system. This mathematic model uses the value of $\chi = 1.26$ [6].

To get an equation which describes the pressure inside the muscle depending on the mass flow, the Equation 3.4 must be differentiated and combined with Equation 3.5 and leads to:

$$\dot{p}_m = \frac{\chi}{V_m}(R_s \cdot T \cdot \dot{m} - p_m \cdot \dot{V}_m)$$

Equation 3.6

The expression inside the brackets describes the flow power. It depends on the mass flow and the change of volume. The temperature T is assumed to be constant.

3.3.4   Air flow through valve

Pneumatic deals with compressible gases as a medium. As it for the evaluation of mass balances in a specified volume like the valve the massflow has to be taken into account. The state variables of the fluid are related to the nominal state which is defined in ISO 6358:

- Temperature in Kelvin $T = 293.15\,K$

- Pressure in bar $p = 1\,bar$

- Humidity in percent $\varphi = 65\%$

- Specific Gas Constant $R_s = 288\dfrac{J}{kg*K}$

The mass flow is generated by a pressure differences between the pressure supply and the pressure in the muscle. The resistance of the valve is very complex because the design is not like an aperture or an injector. Therefore, it is very difficult to define it by a simple mathematic equation. Because of that, it is based on experimental data.

With the help of the conductance value C and the critical pressure rate b, which are given from the manufacturer and are based on experimental data, the massflow can be approximated by the following relation:

$$\dot{m} = C \cdot p_1 \cdot \rho \cdot \sqrt{\frac{T_0}{T_1}} \cdot \begin{cases} \sqrt{1 - \dfrac{\left(\dfrac{p_2}{p_1} - b\right)}{(1-b)}} & , \quad for \quad b \leq \dfrac{p_2}{p_1} \leq 1 \\ 1 & , \quad for \quad 0 \leq \dfrac{p_2}{p_1} \leq b \end{cases}$$

Equation 3.7

- p_1 is the pressure before the valve

- p_2 is the pressure behind the valve

- T_0 Temperature defined in standard state

- T_1 Temperature of the gas before the valve

- ρ density defined in standard state

- C conductance value

- b critical pressure rate

As an application of Equation 3.6 and Equation 3.7, the massflow into and the pressure in a fixed volume is simulated.
As shown in Figure 3-12 sketches.
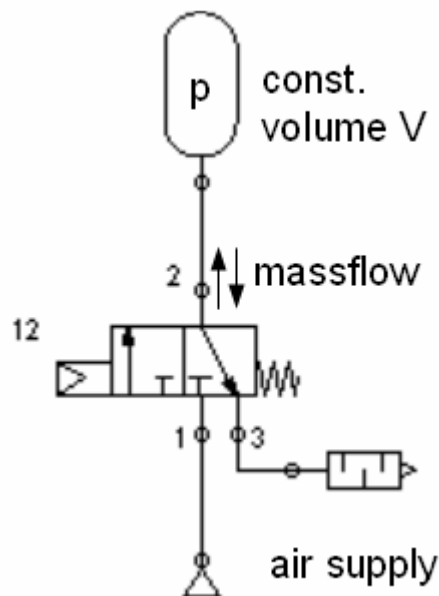
Figure 3-12 Set-up of pressure and massflow simulation

Figure 3-13 shows the massflow between valve and reservoir as well as the pressure in the reservoir.

Figure 3-13 Signals of the pressure and massflow simulation

At line "a" the valve switches and connects the air supply to the constant volume V. The massflow raise up immediately whereas the pressure increases moderately. At line "b" this process is finished. At "c" the valve switches back and the flow out of the volume starts. At "d" the ambient pressure is reached.

3.3.5 Shaft

The shaft has only one degree of freedom. As generalized coordinate the angle α is chosen and the equation of motion follows the Euler's equation.

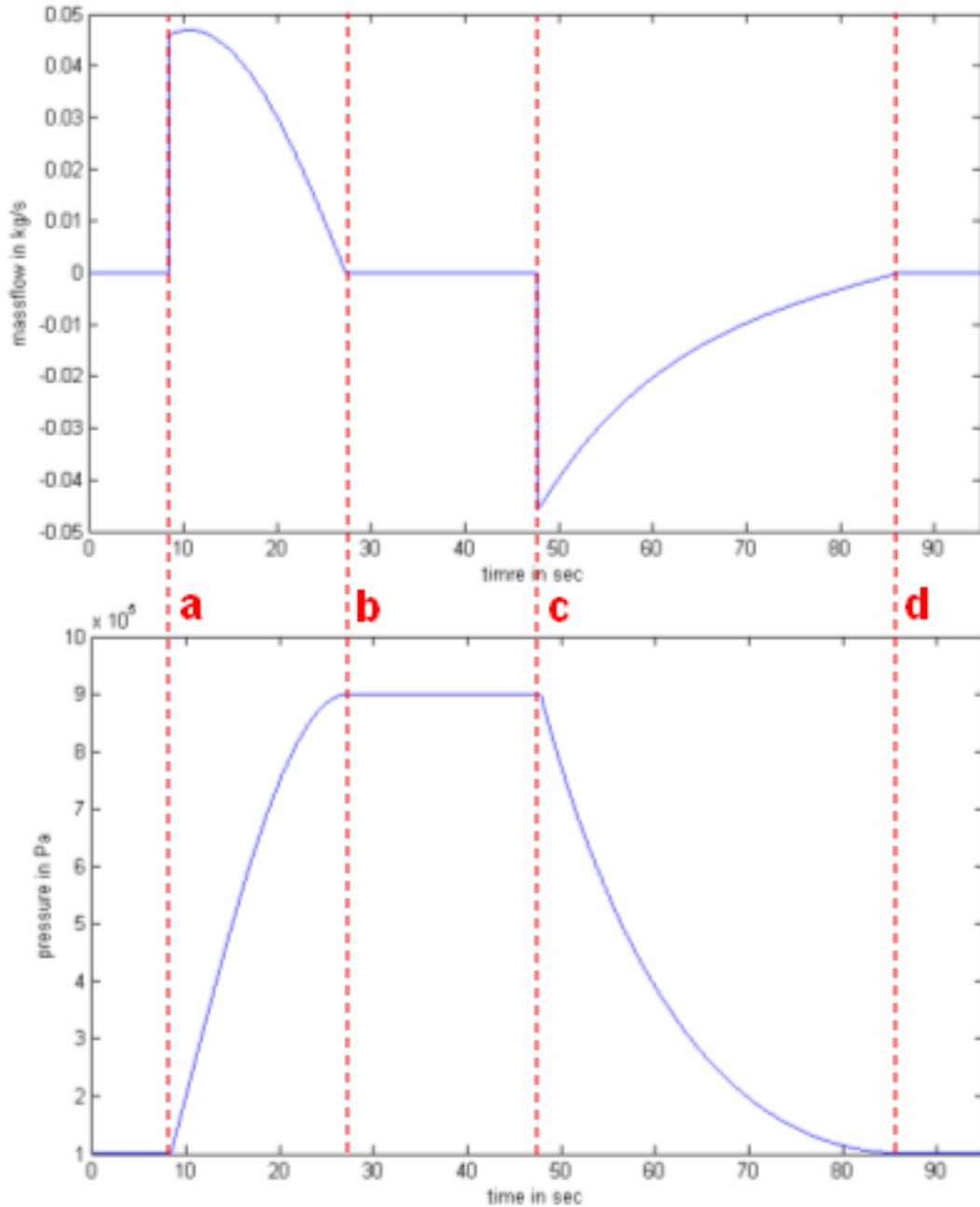The model of the shaft is shown in Figure 3-14 ($\dot{\alpha}$. is chosen in negative direction):
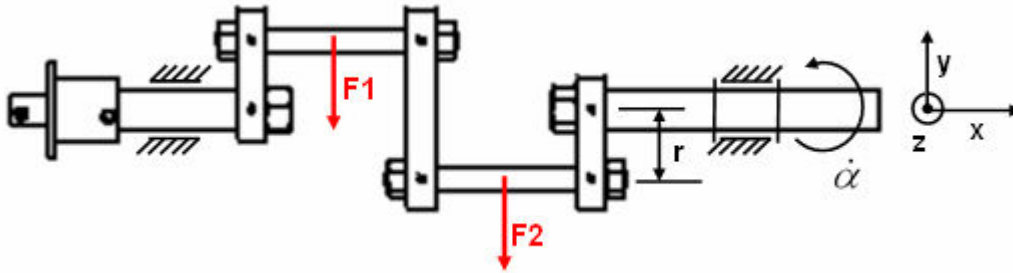
Figure 3-14 Principle draft of the shaft

Setting up the equation results in:

$$I_g \cdot \ddot{\alpha} = F_1 \cdot r \cdot \sin(\alpha) + F_2 \cdot r \cdot \sin(\alpha - \pi)$$

Equation 3.8

$I_g = 55.25\, kg\, cm^2$ is the complete flywheel mass of the shaft inclusive flywheel

$r = 22\, mm$ is the length of the arm. ($2 \cdot r$ defines the maximum stroke)

The state of the shaft defines geometrically the actual stroke of the two muscles and is defined as:

$$s_1 = 22\, mm + 22\, mm \cdot \cos(\alpha)$$
$$s_2 = 22\, mm + 22\, mm \cdot \cos(\alpha - \pi)$$

Equation 3.9

Stroke of muscle 1 is s_1 and of muscle 2 it is s_2. Between them is a phase shift of π. This fact is also seen in Figure 3-15.
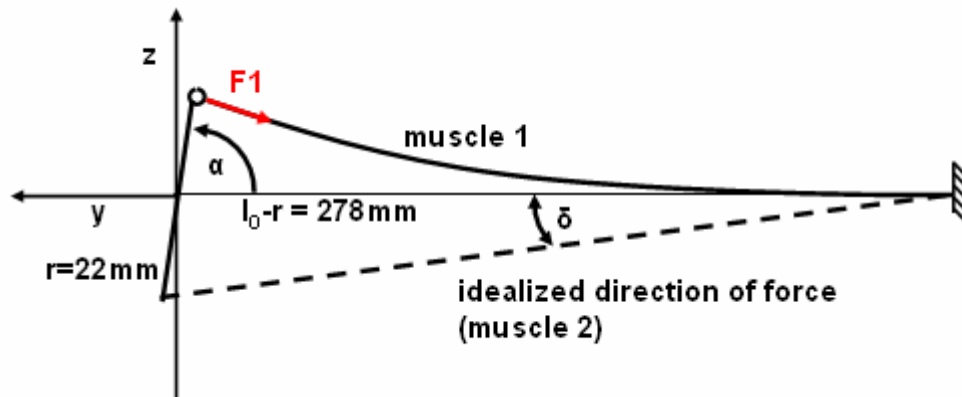
Figure 3-15 Side draft of the shaft

The muscle is connected to the shaft via roller bearing in the connector and has a fixed support to the inertial frame. Figure 3-15 shows the resultant bending in the muscle1 and the idealized orientation of the muscle force (Muscle 2). By the assumption of a long muscle the angle δ can be neglected in the mathematic equations because the result of

$$\sin(\delta_{mas}) = \frac{r}{l_0 - r}$$

Equation 3.10

is very small for $l_0 \gg r$.

4 Experiments

4.1 Vibration Tests

The goal of this experiment is to show the behaviour of the actuators passive damping feature.

One pressurized actuator was displaced by a defined rotation angle $\Delta\alpha$ of the shaft. The second actuator and the flywheel were demounted and had therefore no influence on the system. By an abruptly release, the oscillated speed signal of the shaft was measured. A sketch of the test shows Figure 4-1:
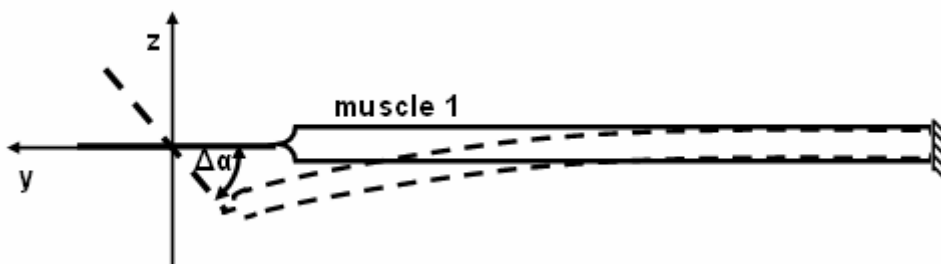
Figure 4-1 Sketch of the vibration test

The muscle acts like an air spring. Figure 4-2 and Figure 4-3 show the recorded speed signals for different pressures and for different initial displacement.

The Nomenclature of the signal names for example p8a40v1 is:

- p8 = 8bar relative pressure in the actuator
- a40 = initial displacement
- v1 = number of experiment

An initial displacement of 20° connotes a contraction of the muscle of 4.33% and 40° of 12.23%.
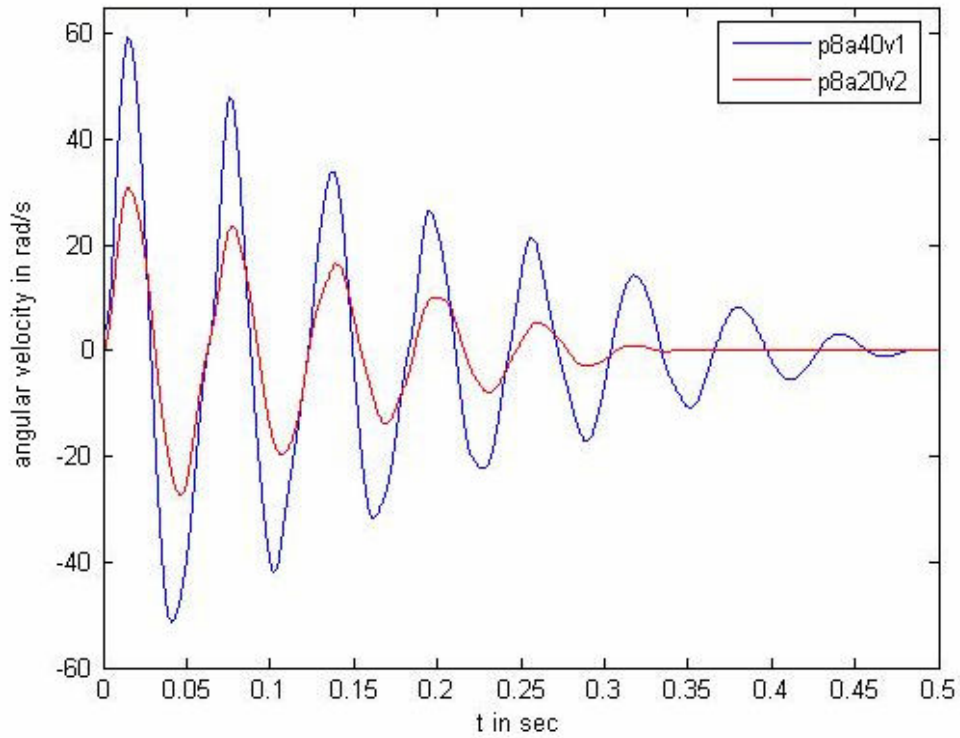
Figure 4-2 Recorded speed signal for 8 bar pressure
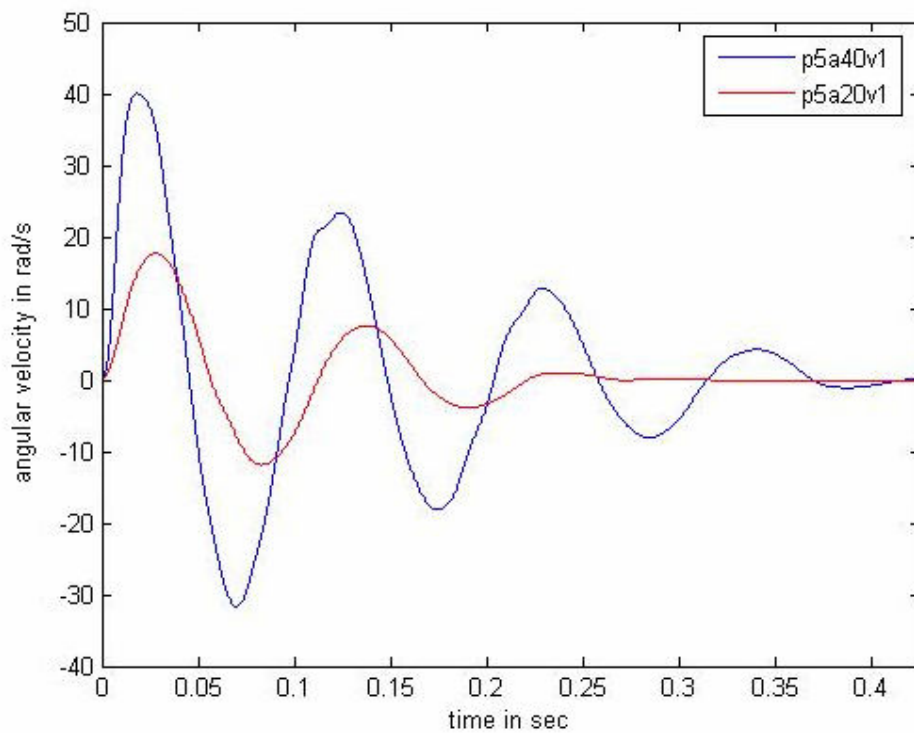
Figure 4-3 Recorded speed signal for 5 bar pressure

It is obvious that the oscillation is more intensive for higher pressure and bigger displacement because of more accumulated energy.

The absorption consists off different parts like the pressurized air, friction for example in the roller bearings and the passive damping of the actuator. It is very difficult to separate these parts. Another not definable part is the unprecisely manufactured shaft and the bending of it.

The damping factor of the oscillation can be identified via the logarithmic decrement. Figure 4-4 shows the p7a40v1 signal after a sudden release.

Figure 4-4 Recorded speed signal for 7bar with ticks

The following calculations are exemplarily done for p7a40v1. The complete results are in Table 4-1.

Logarithmic decrement:

$$\vartheta_{p7a40} = \frac{1}{k}\ln\left(\frac{x_n}{x_{n+1}}\right) = \frac{1}{8}\ln\left(\frac{641.2}{14{,}92}\right) = 0.4701$$

Equation 4.1

Damping factor (modal damping, Lehr):

$$D_{p7a40} = \frac{\vartheta}{\sqrt{4\pi^2 + \vartheta^2}} = \frac{0.4701}{\sqrt{4\pi^2 + 0.4701^2}} = 0.0746$$
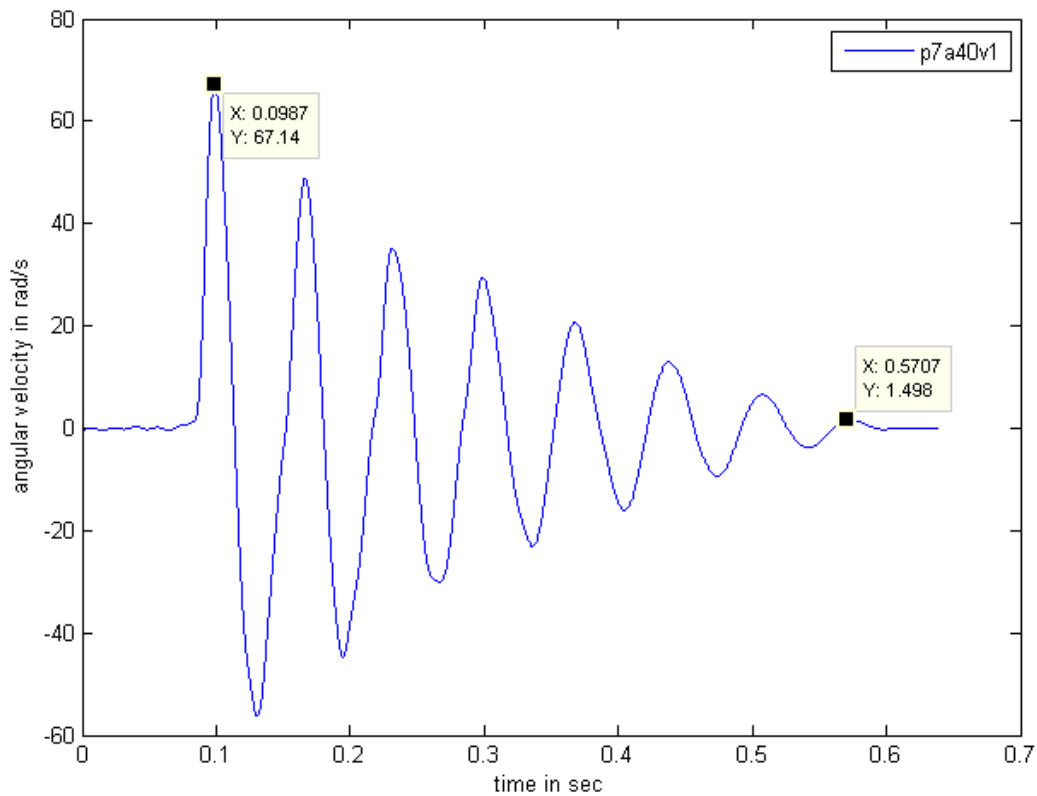
Equation 4.2

Natural frequency:

$$f = \frac{1}{T} = \frac{8}{0.5734s - 0.09889s} = 16.9\,Hz$$

Equation 4.3

Table 4-1 Logarithmic decrement, damping factor and frequency

	P5a20 v1	P5a40 v1	P6a20 v2	P6a40 v3	P7a20 v3	P7a40 v1	P8a20 v2	P8a40 v1
ϑ	1.466	0.746	0.854	0.552	0.503	0.537	0.687	0.422
D	0.227	0.118	0.135	0.088	0.08	0.085	0.109	0.067
f	9.6Hz	9.3Hz	12.1Hz	12.3Hz	14.6Hz	14.8Hz	16.6Hz	16.4Hz

A higher pressure causes a higher stiffness of the system this leads to higher natural frequencies. All signals show at the end of the vibration a sudden stick, which indicates the presence of Coulomb's friction. The influence of this damping mechanism is decreasing for the higher supply pressure.

In Figure 4-3 the blue signal is not a pure harmonic motion. The signal has small bumps, which indicate additional frequencies.

To confirm this statement, a FFT into to the frequency domain was performed and the spectra e.g. for 20°initial displacement are shown in Figure 4-5.
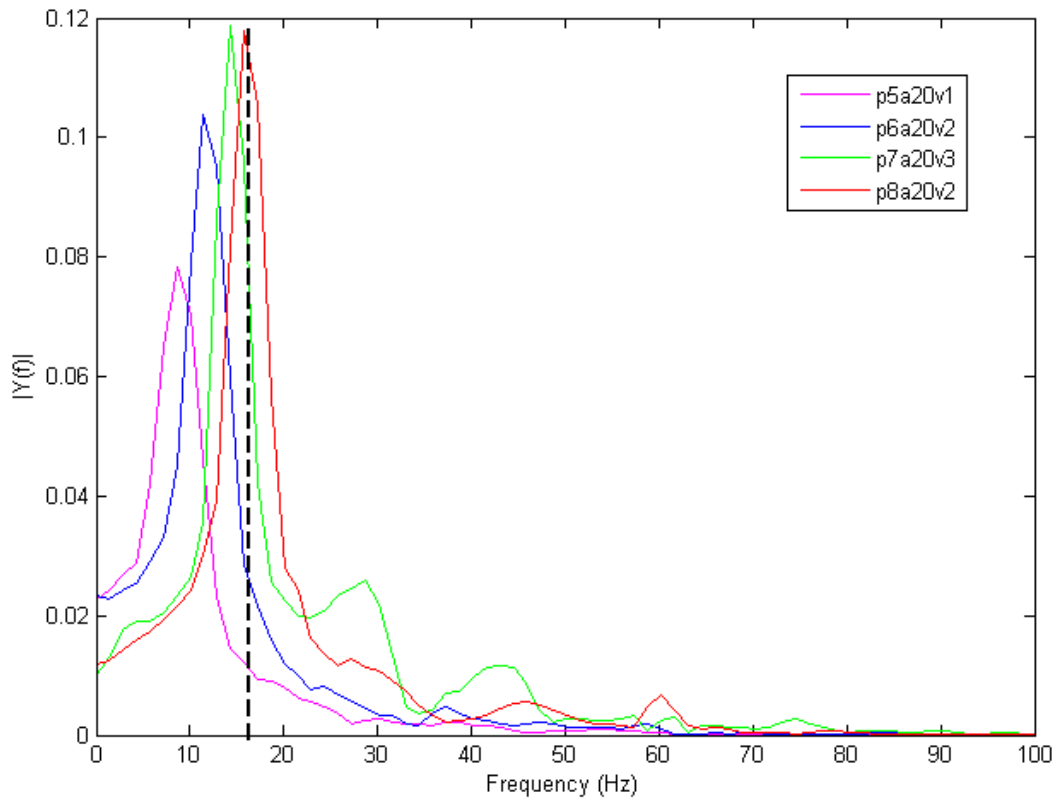
Figure 4-5 Spectra for a displacement of 20°

The spectra show more than one peak. For example, signal p7a20 has the first peak around 14Hz, the second around 28Hz and third around 43Hz. This indicates that higher harmonics are present. A reason for that may be a nonlinear behaviour of the system. It is known that rubber springs, air cushions and friction damping leads to nonlinear characteristics.

4.2 Running Tests

These experiments where executed with the motor, which was introduced in chapter 3.1 and 3.2, under variation of the three input parameters.

First input parameter was the supply pressure. The values for the supply pressure were 5, 6, 7 and 8 bars. Second input parameter was the opening of the flow-control

valve which controls the mass flow. Third input parameter was the set of the switch points. Figure 4-6 shows the how the switch point of the actuators can be set.
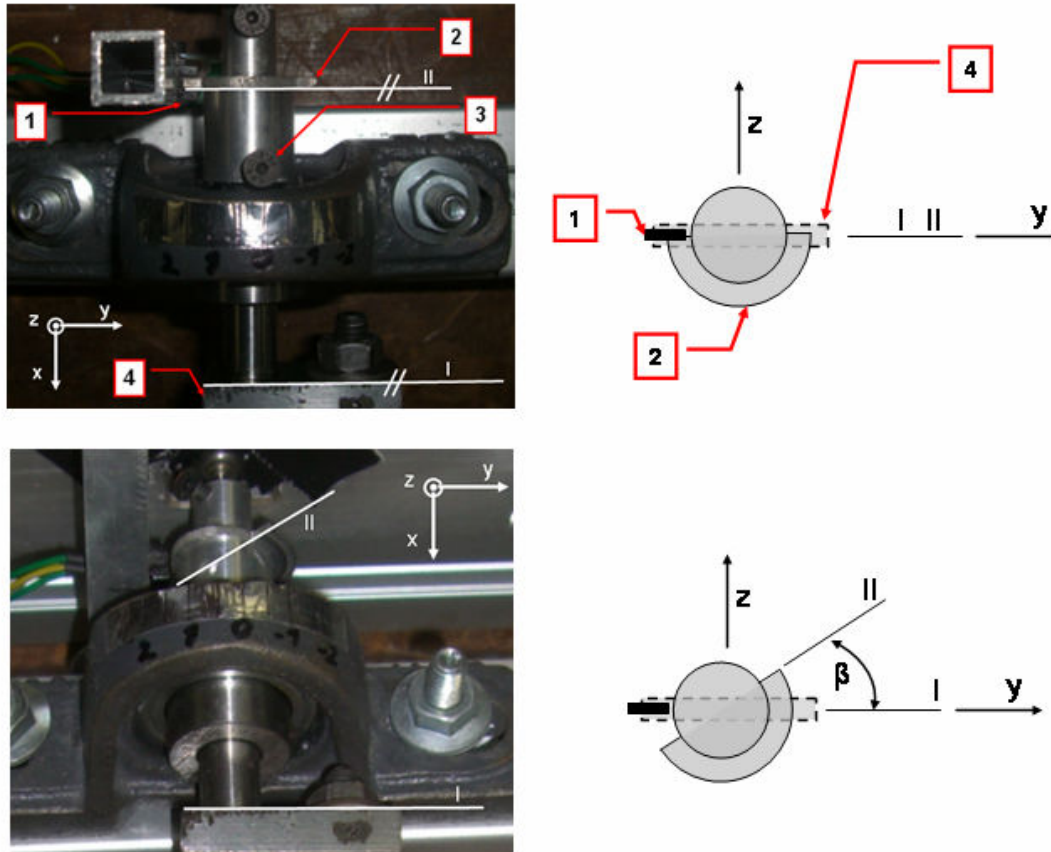
Figure 4-6 Set of switch points

The red tags are:

1. the optocoupler
2. the half disc
3. the set screw to fix the disc
4. the crank shaft

The angle β defines the angle of the pre shifted switch point with respect on the crankshaft. The angle β ranges between 0° and 50°. In the upper half of Figure 4-6 the state for $\beta=0$ and in the lower part the state for $\beta\approx30°$ is shown.

In all experiments the rotation speed of the shaft was measured with a sample rate of 47 kHz.

The files were named by the following nomenclature.

For example: p7a15sp86v1:

- p7 = 7bar relative pressure
- a15 = pre shifted switch point (a = 0-2.5 is equivalent to $\beta = 0° - 80°$)
- sp86 = valve opened with 86%
- v1 = version 1
- acc = acceleration
- ss = steady state
- ro = switch off phase
- f = filtered

4.2.1 Different sections

The motor is started by setting the optocoupler supply voltage from 0V to 5V. It is switched off in the opposite way. Before starting and after switching off the motor the monostable directional valve is holding its initial state, this means one actuator 1 is connected to supply pressure and actuator 2 is connected to the ambience.

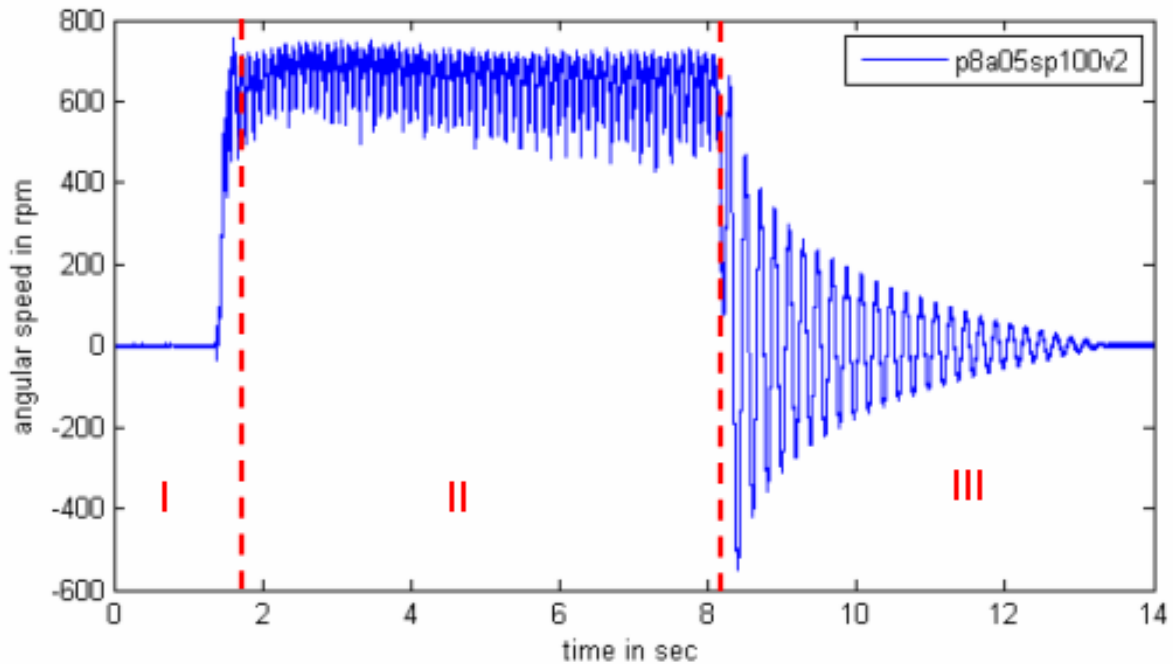Figure 4-7 shows a recorded typical recorded angular speed signal.

Figure 4-7 Recorded angular speed signal

The entire signal can be divided into three sections:

- Acceleration phase.
- Steady state
- Stop phase

These three different parts are detailed studied in the following chapters.

4.2.2 Acceleration Phase

Figure 4-7 shows a high acceleration after starting the motor (section I). The acceleration value depends on the 3 introduced parameters. Every parameter affects the process differently. By a bad combination, the motor starts to turn in negative direction or even oscillate.

The biggest influence has the pressure; the higher it is the faster the motor accelerates. This fact is shown in Figure 4-8.

The signals range from 0 rpm up to around 500 rpm which is near the steady state. They were extracted from the recorded speed signals and were filtered with a cut off frequency of 200Hz.
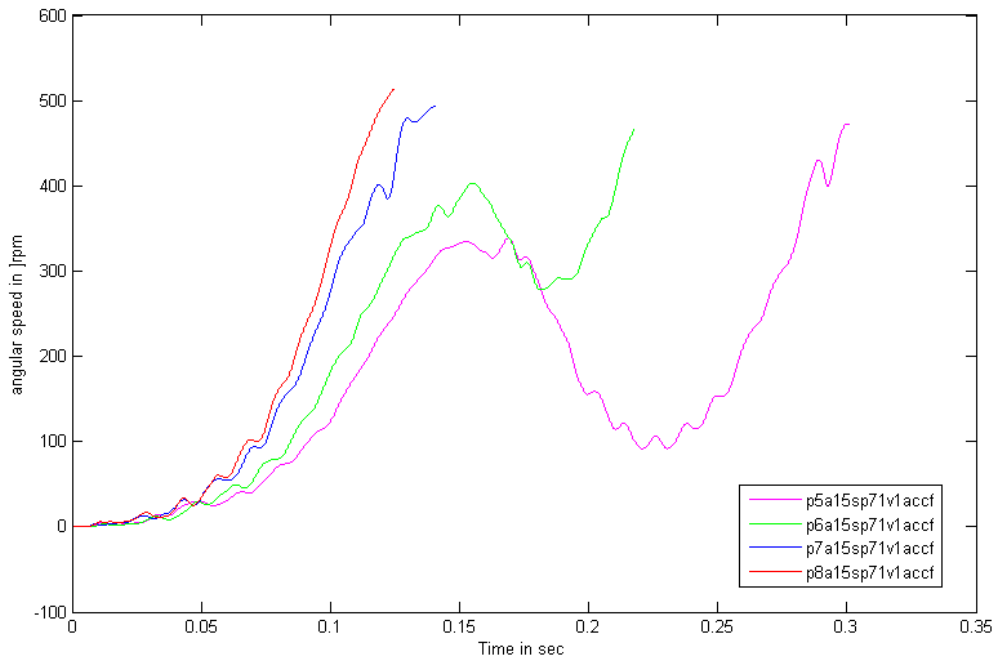
Figure 4-8 Influence of pressure in the acceleration phase

As expected Figure 4-8 shows that the acceleration is growing with a higher pressure. The reason for this it is the actuators force, which depends on the pressure, and was already explained in chapter 2.2.2 and chapter 3.2.1.

The signals for five and six bar are obviously different from the signals with seven or eight bar pressure. This phenomenon is caused by switching between the actuators. With a lower pressure, the motor has less power so it is not able to accelerate the system with one cycle up to 500rpm. A cycle is defined as a half rotation of the shaft between two switchpoints.

The switch characteristic for one pull is detailed checked up by an inspection of the angle of the shaft. This is done by an integration of the recorded angular speed signal. Figure 4-9 shows on the left side in the upper part the angular speed over time and in the lower part the angle over time. The ride side shows sketches of the state of the shaft for certain times.
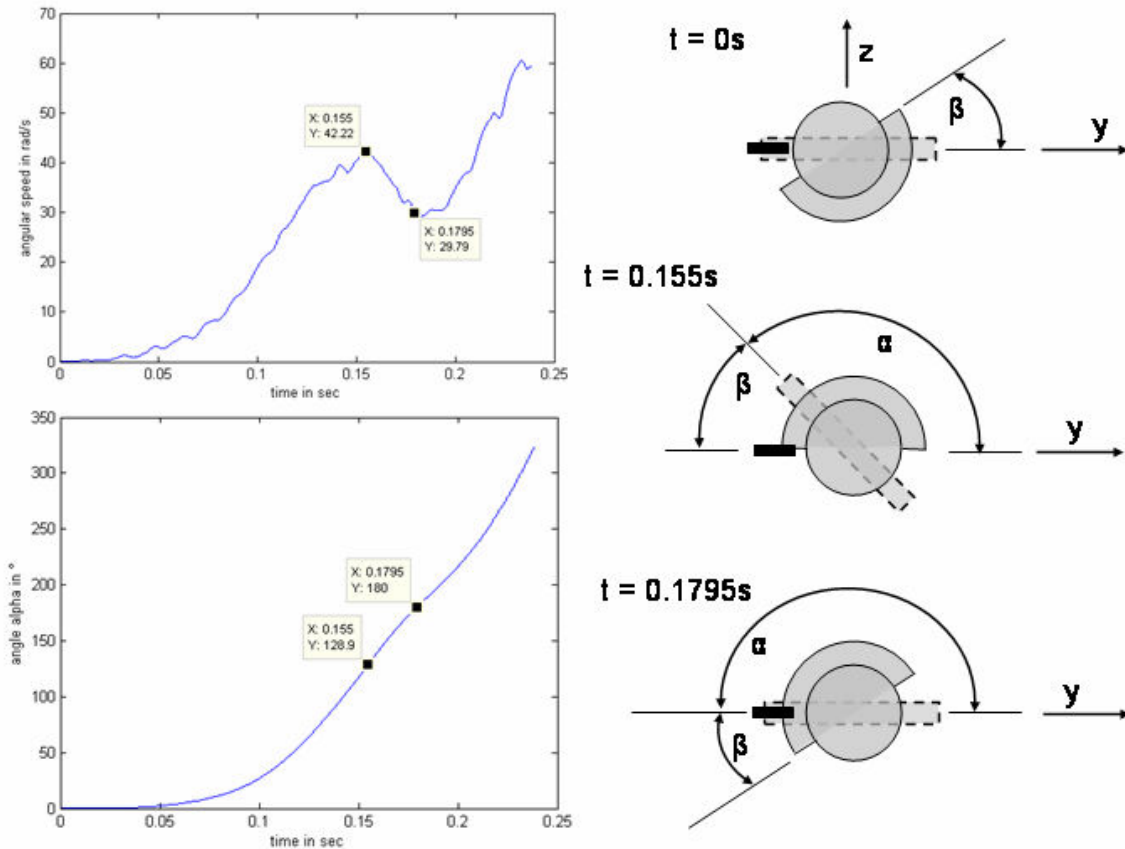
Figure 4-9 Switch characteristic of a cycle

For $t=0s$ the shaft has its initial state $\alpha=0°$. At $t=0.155s$ the system is switching and the state of the shaft is $\alpha=129.9°$ consequently the pre shifted angle is $\beta=31.1°$. Up to $t=0.1795s$ a negative acceleration is identifiable. At this time the shaft reaches $\alpha=180°$ and the acceleration change into a positive value.

The influence of the flow-control valve is shown in Figure 4-10, exemplary with the setting of 8 bar pressure and a pre shifted angle of 34°. All signals were filtered and extracted of the recorded speed signal up to a time of $t=0.163\,s$. This is the time when signal p8a1sp100v1 has its second switch point.
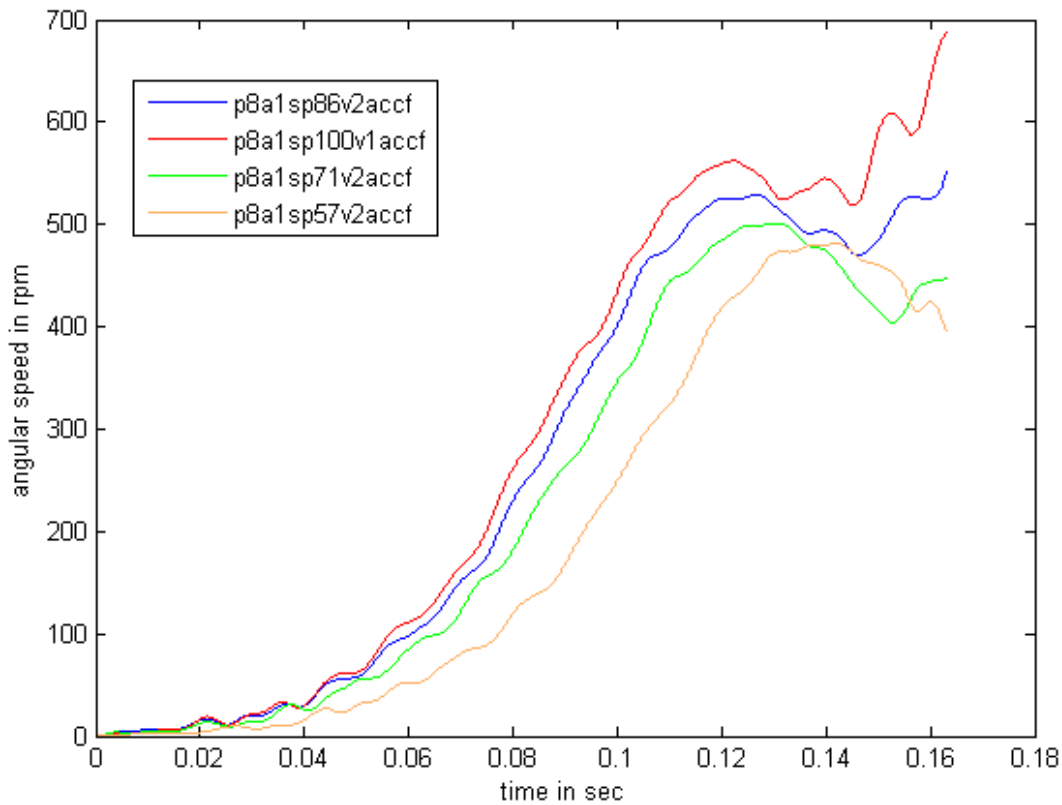
Figure 4-10 Influence of the flow-control valve in the acceleration phase

As expected is the acceleration faster with a more open flow-control valve. Caused by a quicker pressure evolution in the actuator.

4.2.3 Steady State Phase

This chapter describes the steady state of the motor, which is shown in Figure 4-7 section II. The steady state behaviour is characterised by the mean value of speed ω_0 superposed by nonuniform ripples $\Delta\omega$ caused by the switching between the two actuators.

Figure 4-11 Description of ω_0 and $\Delta\omega$

The influence of pressure in the actuators and the spindle position on ω_0 is shown in Figure 4-12. A higher pressure causes a higher mean angular speed. This has two reasons. First, the actuator generates higher forces with higher pressures. Second, a higher pressure difference between the air supply to actuator and actuator to ambient, causes a bigger air flow.
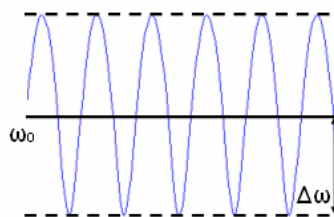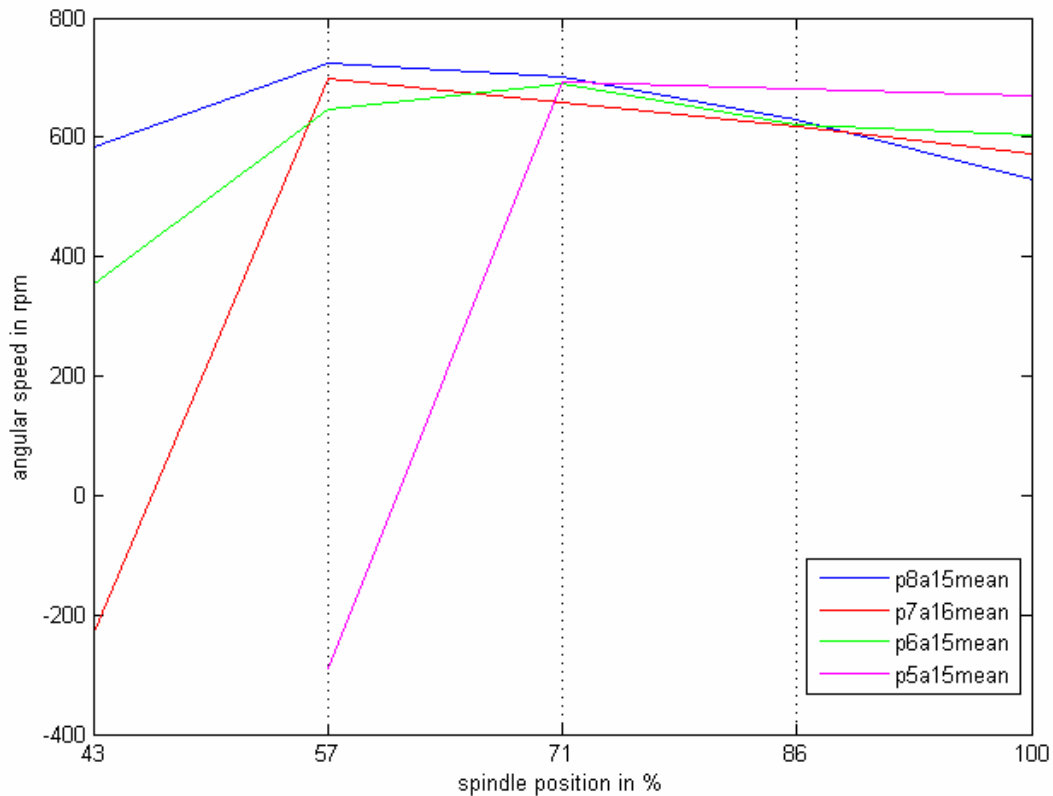

Figure 4-12 ω_0 **depending on the spindle position under different pressures**

The spindle position of the flow-control valve has an interesting influence on ω_0. A reduced opening leads opening leads to a higher ω_0 when the opening is set between 57% -100% and ω_0 drops down drastically when the opening is reduced below 57%.

This phenomenon can also be seen in Figure 4-13, where the rotation speed is plotted depending on the spindle position and the pre shifted angle β.
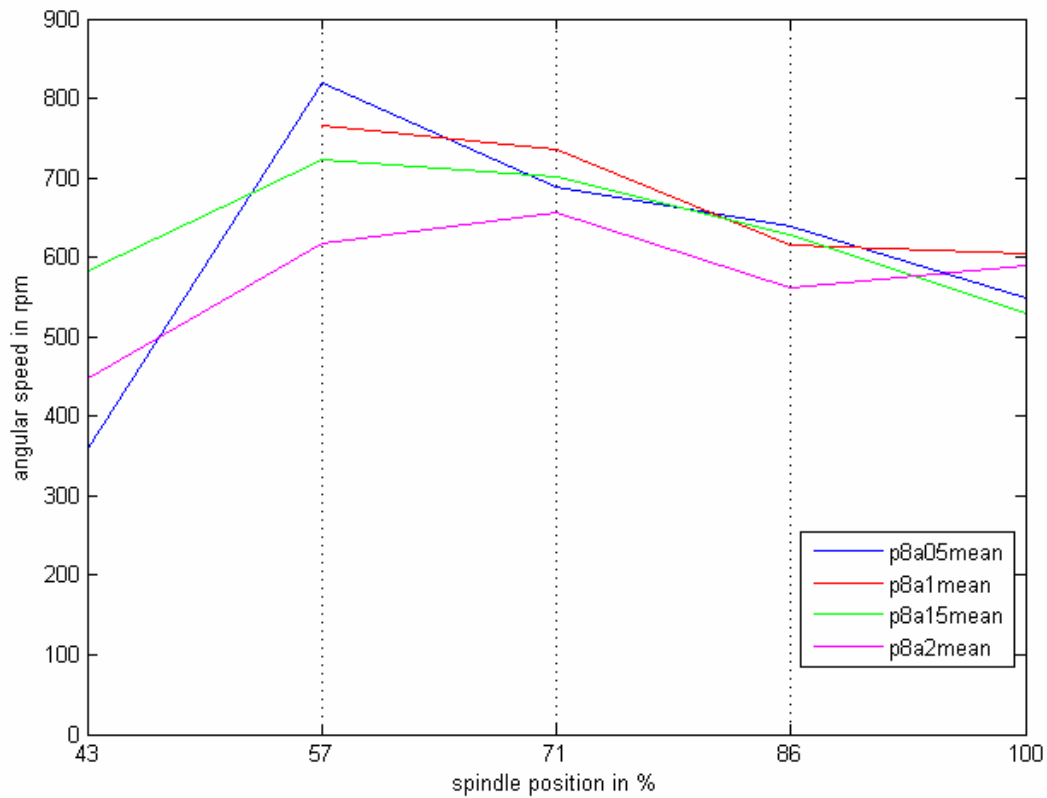
Figure 4-13 ω_0 **depending on the spindle position under different pre shifted angles**

The maximum rotation speed is around 57% of opening and $\beta = 17°$.

The phenomenon of a lower rotation speed at a bigger opening of the throttle can be explained by looking at the input - / output air flow of the actuators and the pressure in the actuators. The input air flow is governed by the adjustable flow-control valve and the pressure difference between the supply and the actuator. The value of the output air flow depends only on the pressure difference between actuator and ambient. The flow resistance in the system is not considered here.

Figure 4-14 shows qualitatively the pressure evolution in the two actuators over the time during a running motor, neglecting the dead beat time and a pre shifted angle.

Figure 4-14 Relative pressure of the actuators over time

Before the first switchpoint of the valve, actuator1 (blue) is in contracting state and its pressure is the supply pressure p_s. After switching the pressure goes down to the ambient pressure p_n.
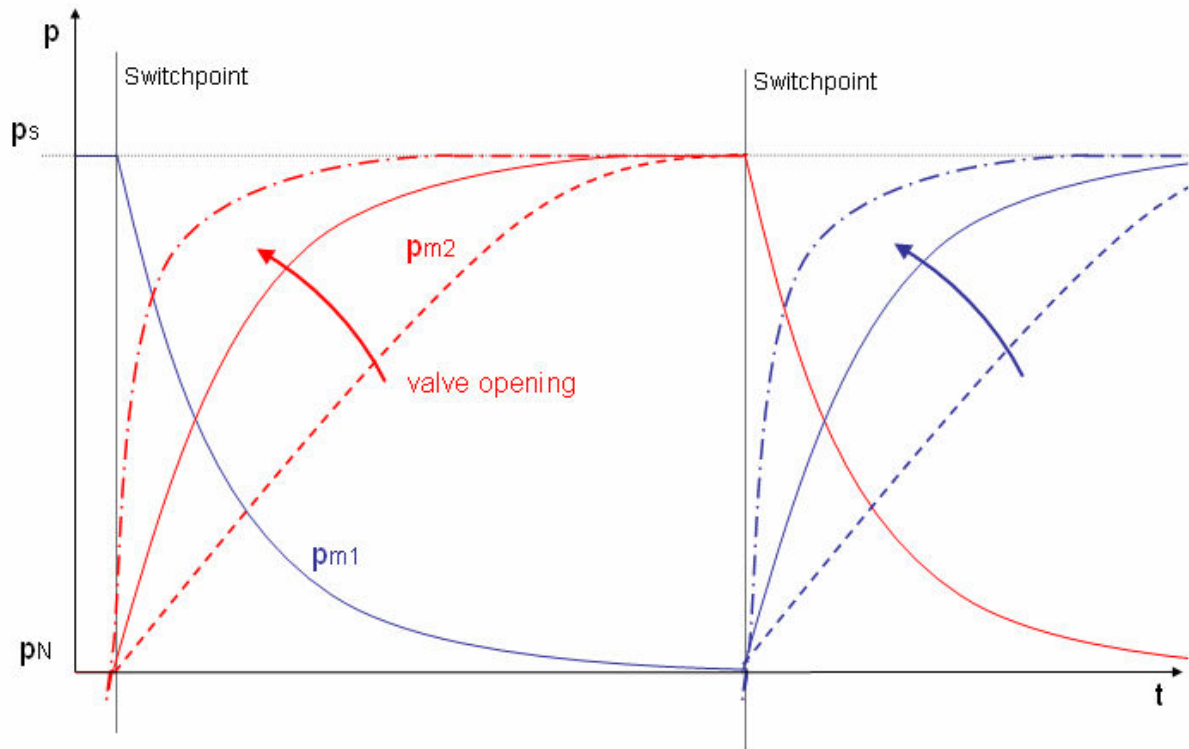
Actuator 2 (red) contracts after the first switchpoint. The evolution of the pressure in the actuator p_{m2} depends on the spindle position. For a smaller opening the pressure grows slower than for a bigger opening. Therefore the time instance, where the pressure in both muscles are equal, is depending on the opening. As long both actuators under pressure they are working against each other. The shorter this time interval the smaller is the work of the actuators against each other.

This effect of working against each other is the reason for the non-uniformity $\Delta\omega$. The degree of non-uniformity is defined as Equation 4.4 and shown in Figure 4-15 and Figure 4-16.

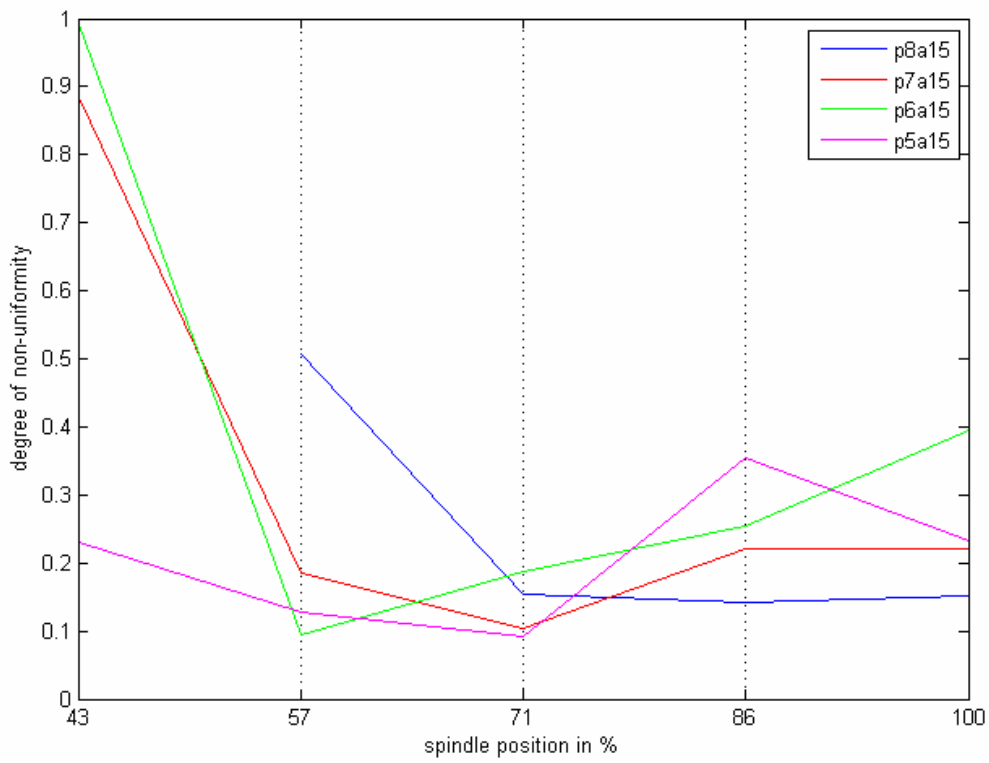$$\lambda = \frac{\Delta\omega}{\omega_0}$$

Equation 4.4

Figure 4-15 Degree of uniformity depending on the pressure
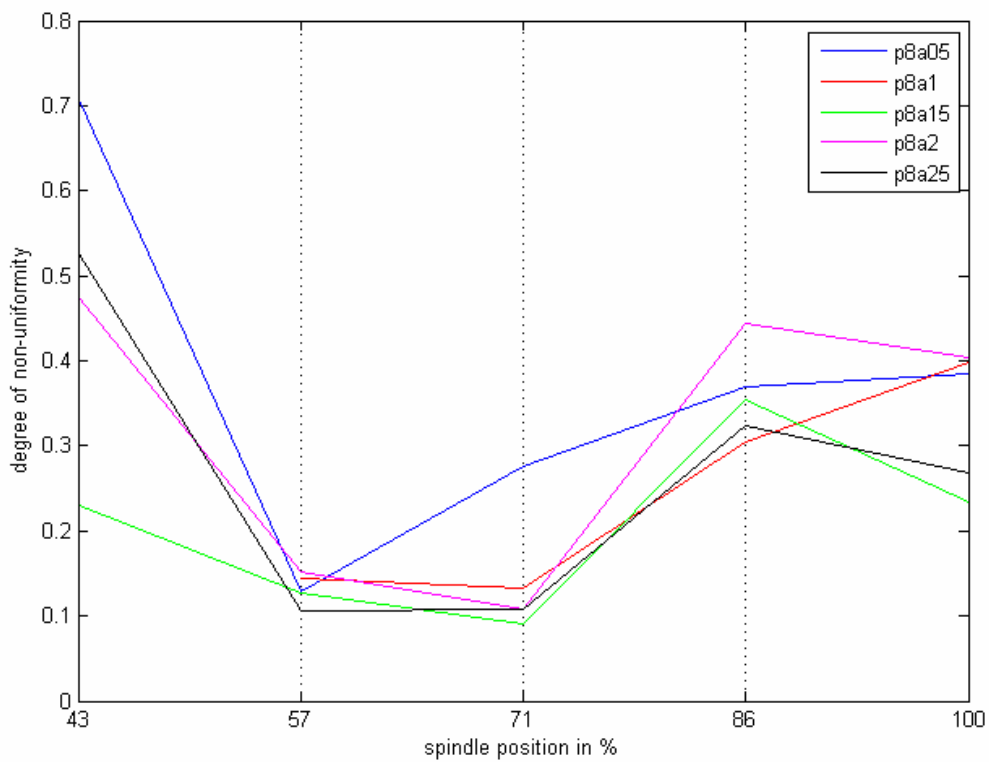

Figure 4-16 Degree of uniformity depending on the pre shifted angle

Between 57% and 71% of opening, the motor shows its smoothest rotation. This is the range, where the motor has its highest rotation speed.

Remark: Additional influence factors for non-uniform rotation are vibrations like transversal vibrations of the muscles, bending of the crank shaft due to high muscle forces and misaligned cranks of the shaft.

4.2.4 Switch off Phase

Section III of Figure 4-7 shows the run-out phase, which begins with turning off the motor. This means that the electric supply of the optocoupler is interrupted and that the valve falls in its initial state: actuator 1 stays is connected to the supply pressure and actuator 2 is connected to ambience. The time instance of switching off is arbitrary related to the crank shaft angle.

Unlike to chapter 4.1, the system vibrates longer, because of the flywheel which was not present in chapter 4.1, acts as an energy storage.
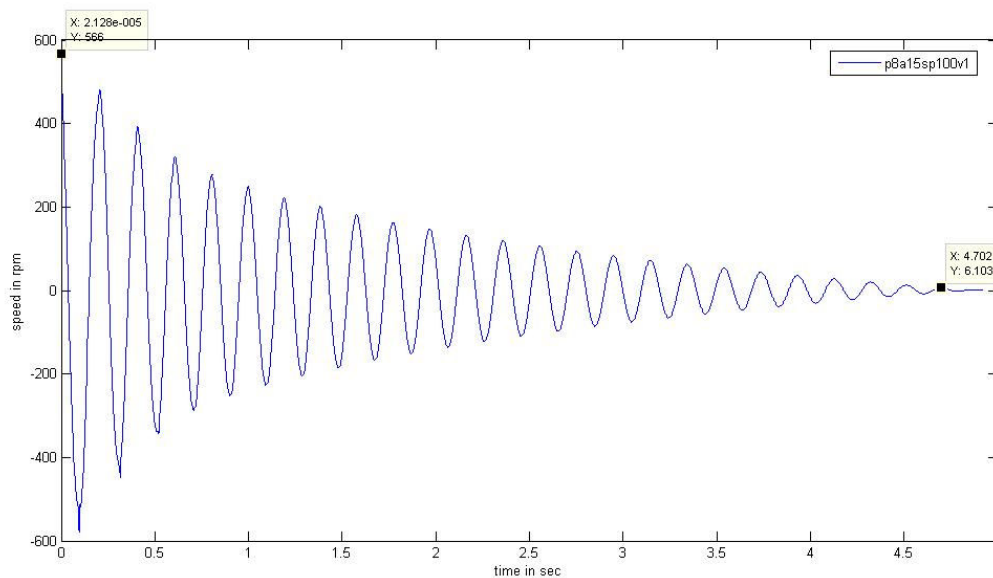
Figure 4-17 Signal of the switch-off phase

In comparison to the results in chapter 4.1 the decay of amplitudes are quite similar to an exponential function. Obviously the friction problem doesn't play an important role.

Analog to the calculation in chapter 4.1, Table 4-2 shows the damping factor and the frequency under different pressure. As expected the natural frequencies and damping factors are lower due to the higher vibration mass of the system.

Table 4-2 Logarithmic decrement, damping factor and frequency in the switch-off phase

	P5a15sp100v2	P6a15sp100v1	P7a15sp100v1	P8a15sp100v1
ϑ	0.2493	0.2082	0.1958	0.1880
D	0.0397	0.0331	0.0311	0.0299
f	3.3Hz	4.1Hz	4.5Hz	5.1Hz

5 Simulation

The simulation with Matlab/Simulink is done to validate the models chapter § and to compare the results of the experiments.

5.1 Set up in Matlab/Simulink

The simulation of the motor was built in Matlab/Simulink, which is a powerful mathematic and simulation tool. The main objective was the simulation of the mathematic models found in chapter 3.3.

One requirement was to build up the block diagram in Simulink with the help of Matlab functions. The block diagram of the motor is shown in Figure 5-1.

The orange blocks are "Matlab Functions" and they are representing the several mathematic sub functions of the motor. The green blocks are "Simout Blocks". They save the results in arrays for further analysis in Matlab. The red blocks are "Continuous Blocks". The simulation uses "Integrator" and "Derivate" blocks. The yellow blocks are the input constants.
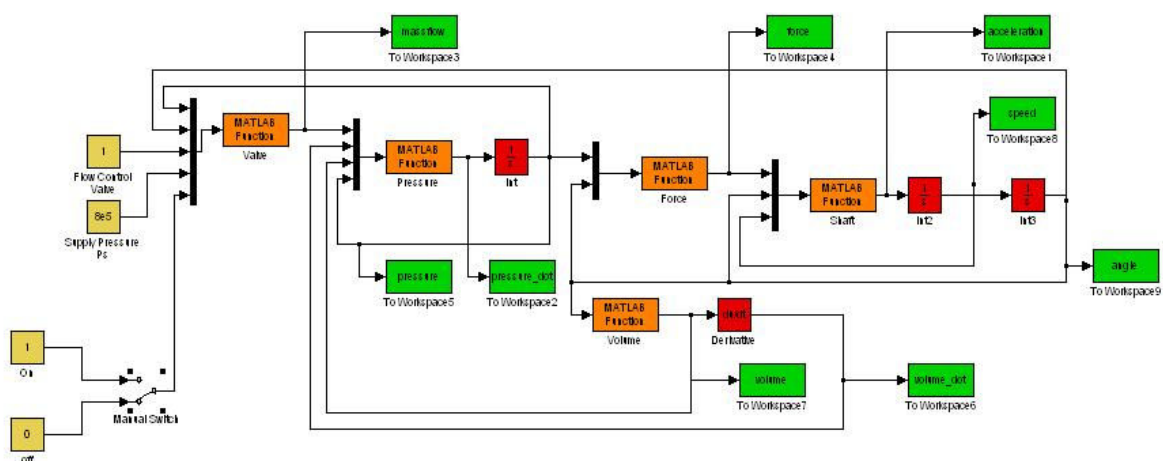

Figure 5-1 Block diagramm of the simulation of the motor

All needed parameters like the ambient pressure, simulation time or the flywheel mass are defined by init "M-Function". All "M-Files" are included in the appendix.

5.2 Simplifications

The electric circuit is not explicit implemented. It is logical programmed in the Matlab Files. Different to the real motor in the simulation the adjustment of the switchpoints is not implemented, the switchpoints are set to 0 and π. The simulation model does not include transversal oscillations like shown in Picture 5-1.
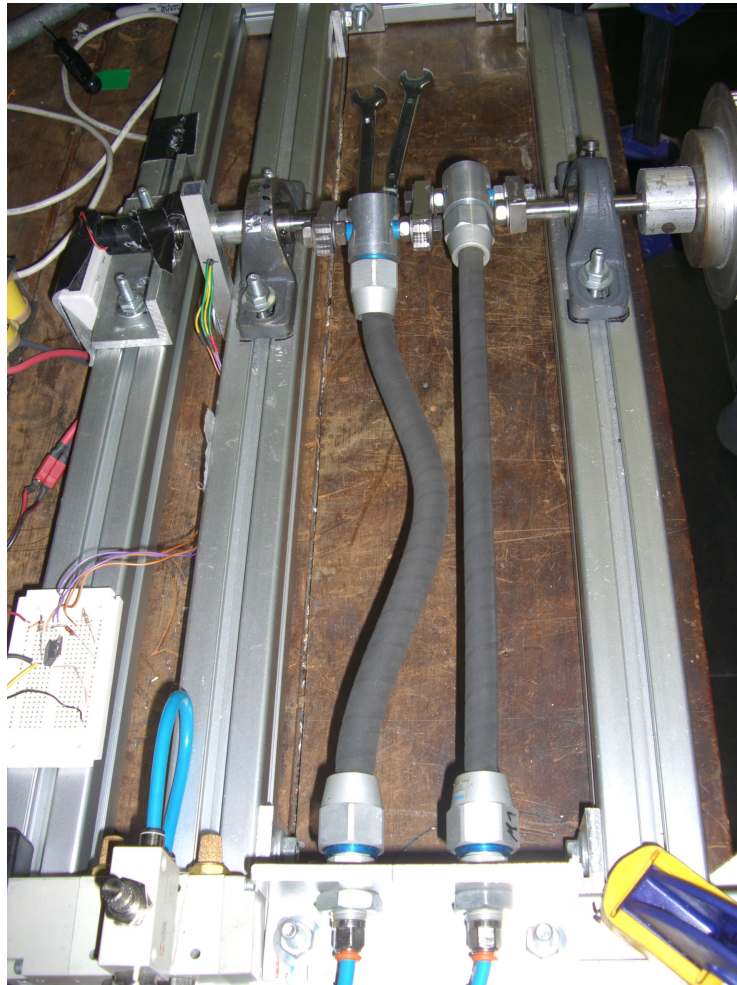
Picture 5-1 Transversal oscillations of the actuator

In Chapter 4 it is shown that damping is not a fixed value, but depending on conditions of operation. In the simulation a fixed value $d = 0.035$ is used which is the mean value of the Table 4-2.

Also not implemented are the pneumatic pipes and the interaction of the supply pressure to the system. The supply pressure in the simulation is constant.

5.3 Speed Test Simulation

This chapter shows the results of the simulation and compares them with the result of the experiments described in chapter 4.2. The acceleration phase (section I), the steady state phase (section II) and the switch off phase (section III) are analog to the results shown in chapter 4.2.
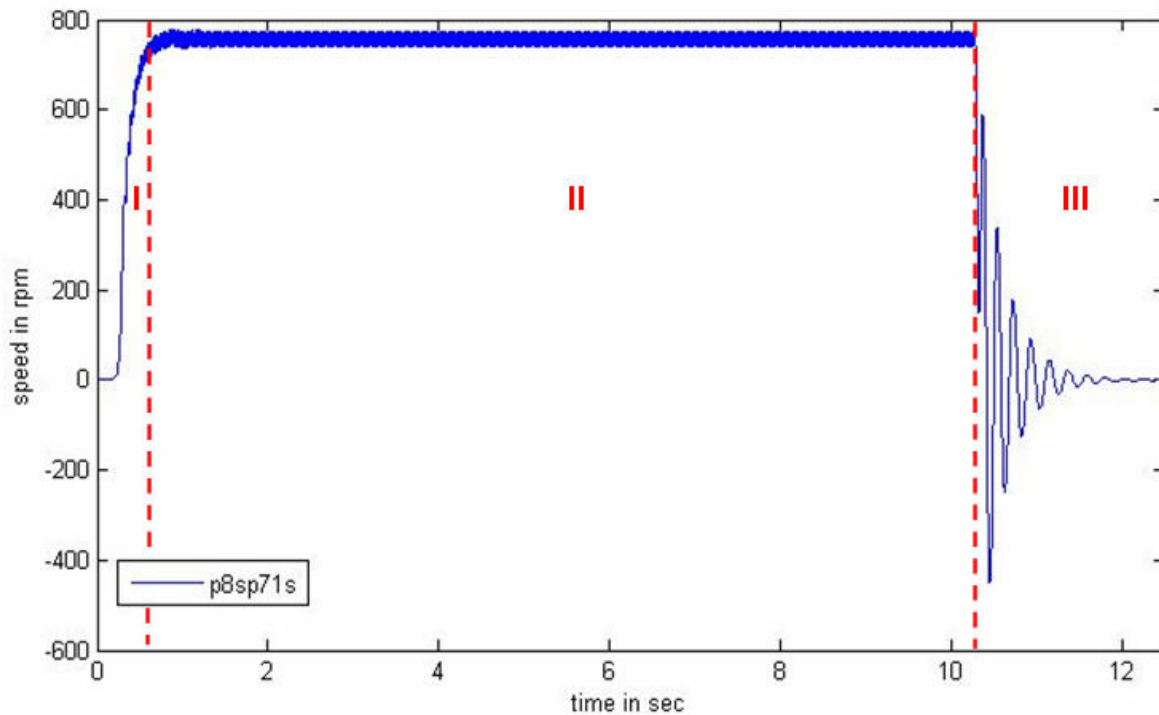
Figure 5-2 Simulated speed signal with the 3 sections

Section I-III are analyzed in the following three chapters in the same way as they were analyzed in chapter 4.2

5.3.1   Acceleration Phase Simulation

In the acceleration phase, the influences of the input parameters pressure and valve opening are determined. Figure 5-3 shows the influence of the pressure. For a higher pressure, the motor accelerates faster than with less pressure. The simulated behaviour of the system up to the first switching points is qualitatively similar to the experiments.

Figure 5-3 Influence of the pressure in the acceleration phase of the simulation

Interesting is that the simulation needs more cycles of the actuators to reach the steady state. For example to reach the velocity of 500rpm the number of cycles differs from simulation to measurement as shown in Table 5-1.
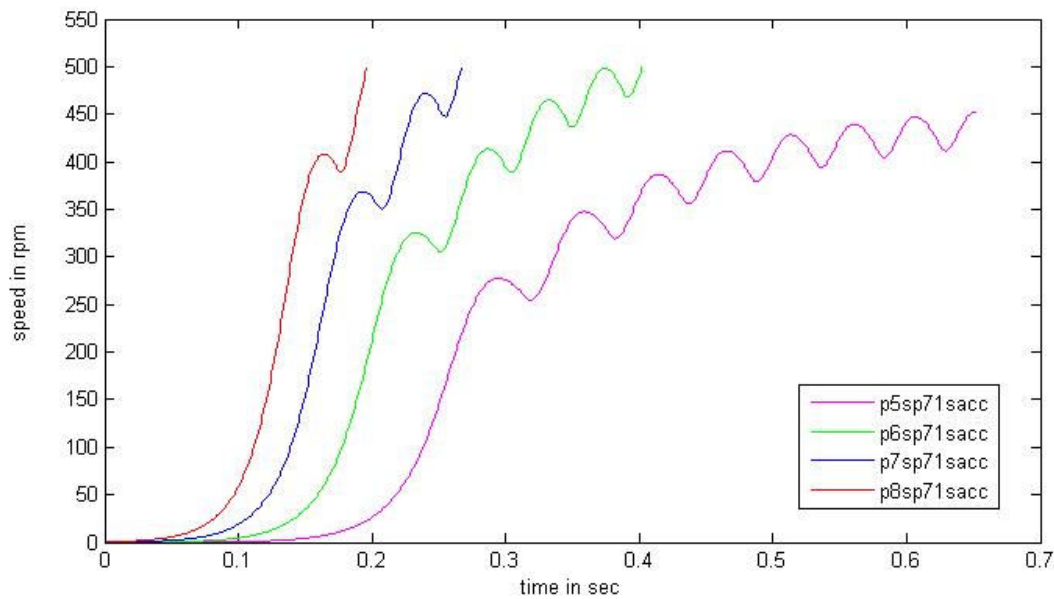
Table 5-1Cycles to reach 500 rpm of the simulation and experiment

	5 bar	6 bar	7 bar	8 bar
Cycles in Simulation	∞	4	2	1
Cycles in Experiment	1	1	0	0

In the simulation the variation of the massflow is realized by a multiplication of the massflow with a factor of reduction. The results of the simulation show that in contrary to the opening of the valve there is no big influence of this factor on the behavior of the motor, see Figure 5-4.

The conclusion is therefore, that the position of spindle (%) is not proportional to the factor of reduction, it is a nonlinear relationship.
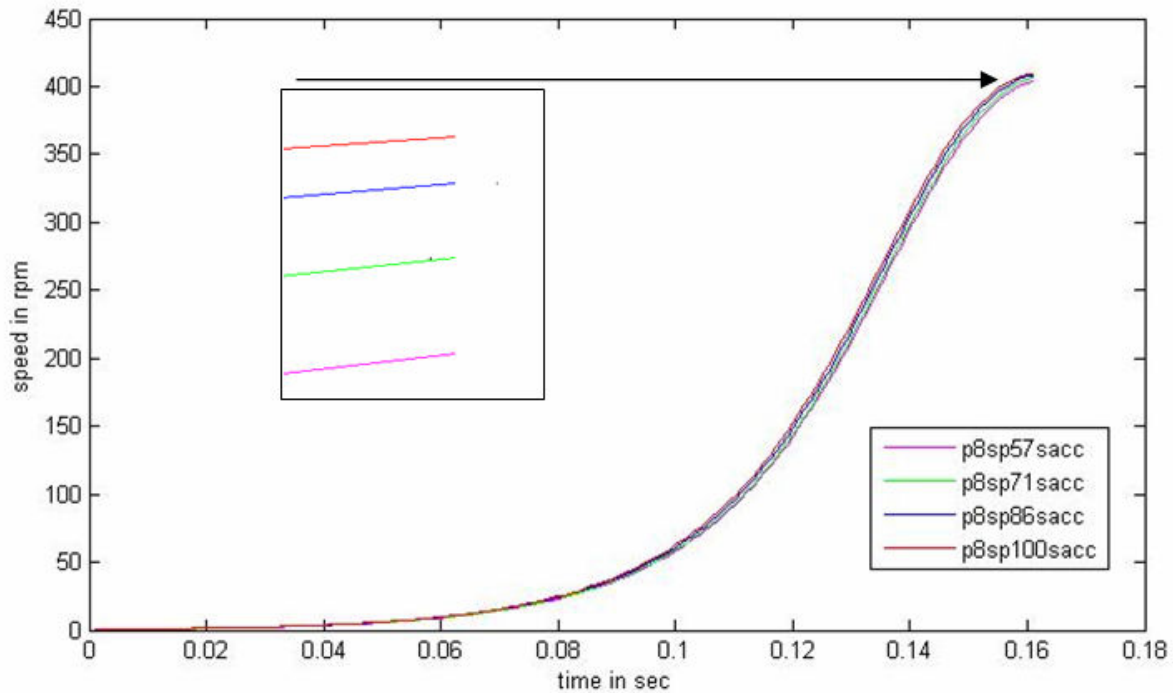
Figure 5-4 Influence of the flow-control valve in the acceleration phase of the simulation

The nonlinear relationship can be seen by checking the angular speed at a certain time instance ($t = 0.16s$).

Table 5-2 Comparison of the angular speed between simulation and experiment at t = 0.16s

Simulation	Factor of reduction	0.57	0.71	0.86	1
	Angular speed in rpm	404.2	406.5	408.3	409.4
Experiment	Spindle position	57%	71%	86%	100%
	Angular speed in rpm	396.6	446.8	552.1	688.5

5.3.2   Steady State Phase Simulation

The steady state behavior in the simulation is quite different to that of the real motor. This is due to the ideal condition and neglecting all disturbances. The mean value ω_0 is governed by the choice of damping which determines the moment of resistance, see Figure 5-5. The non-uniformity $\Delta\omega$ is small and there are no additional variations as shown in Figure 5-6.
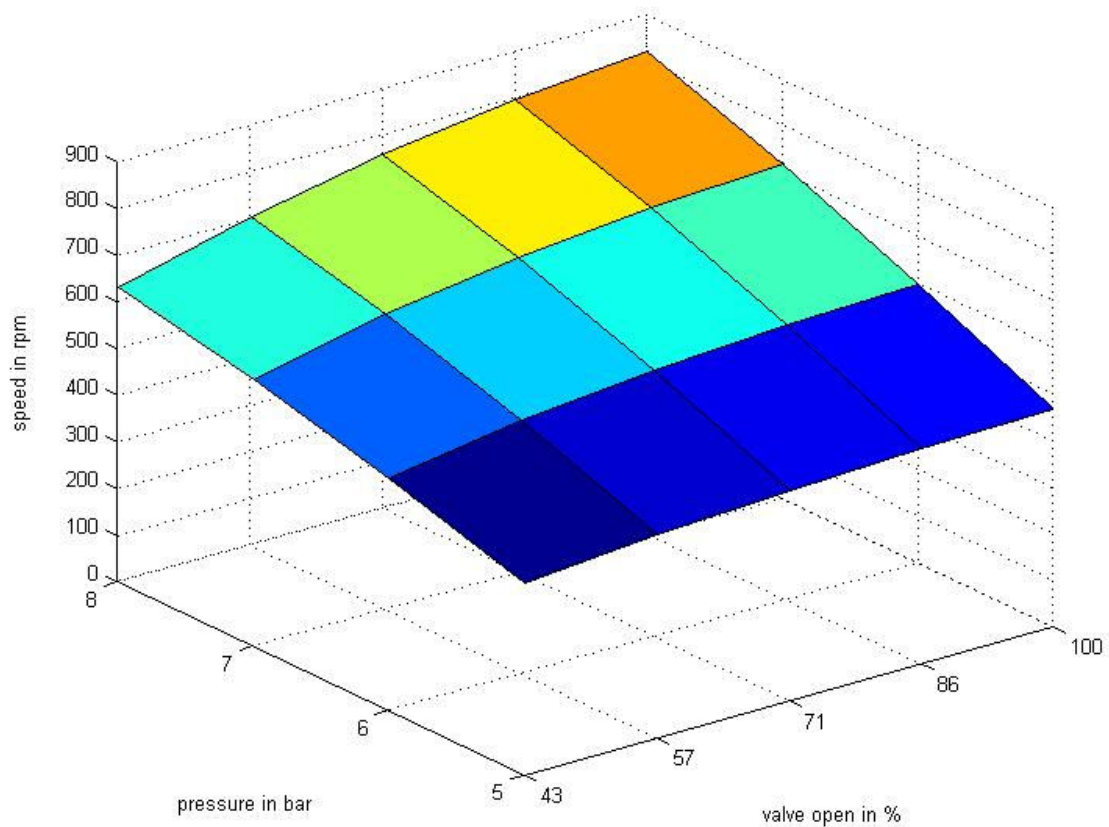
Figure 5-5 Mean rotation speed depending on pressure and spindle position

Table 5-3 clarifies the different results of the spindle position between the simulations and the experiments. This behavior was caused by the characteristics of the massflow. Chapter 5.4.1 shows a detailed description.

Table 5-3 Comparison of the mean angular speed of the simulation and experiment

Simulation (p8)	Factor of reduction	0.43	0.57	0.71	0.86	1
	Angular speed in rpm	632	705	759	798	822
Experiment (p8a05)	spindle position	43%	57%	71%	86%	100%
	Angular speed in rpm	359	819	689	639	548

Figure 5-6 shows the degree of uniformity depending on the pressure and the spindle position. With a higher pressure and a high spindle position the simulated motor

rotates smoother. In opposite to the real motor, the simulated motor runs over ten times smoother.
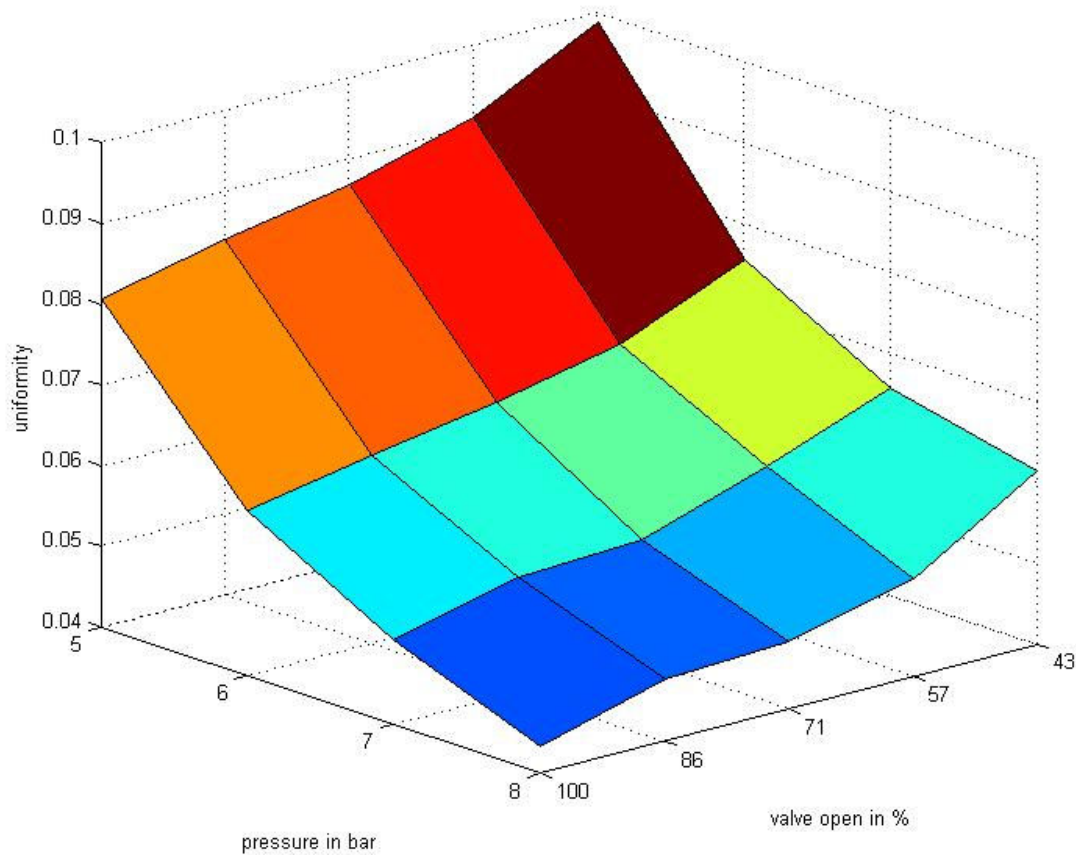

Figure 5-6 Degree of non-uniformity depending on pressure and spindle position

5.3.3 Switch-off phase

In the switch.off phase, the simulated motor shows almost the same behavior as the real motor. Figure 5-7 shows the speed signal of the switch-off phase. In comparison to the recorded experimental angular speed signal the simulated signal decays faster.
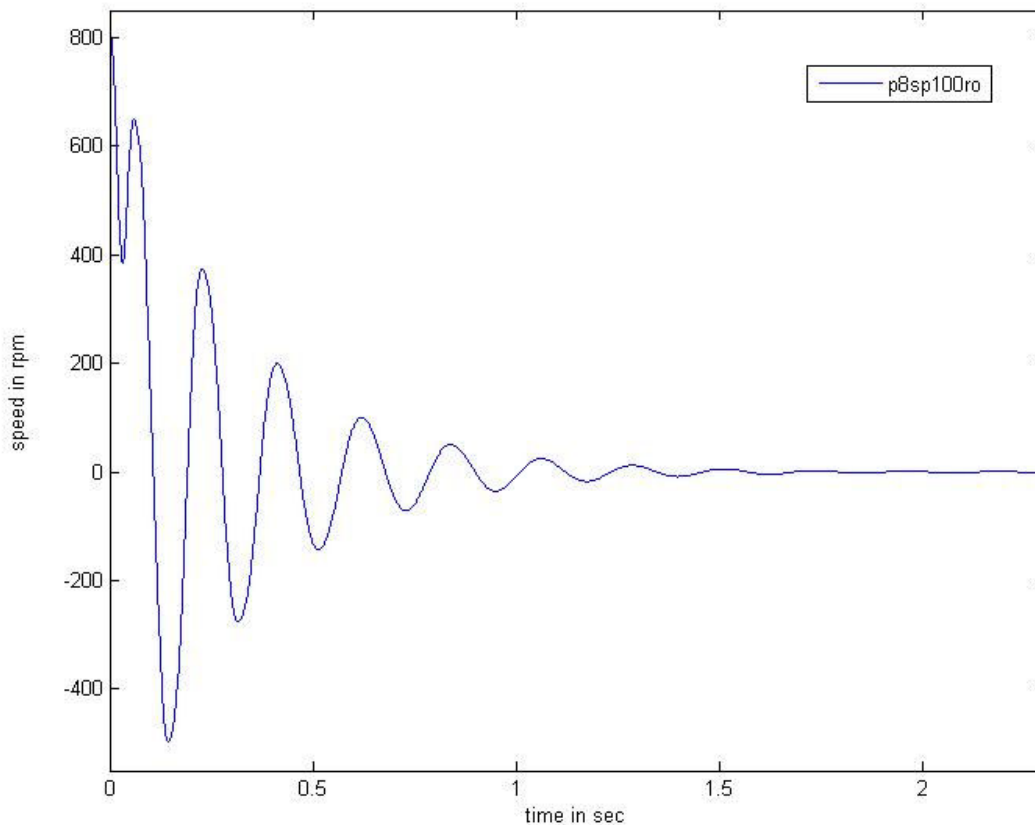
Figure 5-7 Switch-off phase of the simulation

Another effect can be seen in this specific recording at the beginning of switching-off phase. Obviously, the time instance of switching off was close before the point of return $\alpha = \pi$. Due to the kinetic energy of the system the angular velocity remains still positive and the following vibration is around $\alpha = 0$.

Table 5-4 shows the values analog to chapter 4.2.4.

Table 5-4 Logarithmic decrement, damping factor and frequency
in the switch-off phase of the simulation

	P5sp100v1sro	P6sp100v1sro	P7sp100v1sro	P8sp100v1sro
ϑ	0.9070	0.7537	0.6594	0.6012
D	0.1429	0.1191	0.1044	0.0953
f	3.6364	4.3478	4.9080	5.3731

It turns out that the globally chosen damping factor $d = 0.35$ is too high for the switch-off phase.

5.4 Simulation Components

The simulation offers the opportunity to observe other signals like the massflow, the pressure in the actuators and the force generated by the actuators. This chapter analyzes shortly these three signals under different parameters. Actuator one and two are distinguished with the red and blue colour of the simulated signals. In each case of the following figures an interval of two cycles during the steady state is figured out.

The plots from the left to the right and from the top down are belonging to: p5sp43, p5sp100, p8sp43 and p8sp100.

5.4.1   Massflow

Figure 5-8 shows the massflow, where the positive y-axis signifies the input massflow and the negative axis the output massflow.

The output massflow is depending on the difference between the pressure in the muscle and the ambience. The input massflow is depending on the difference between the supply pressure and the muscle pressure and additionally on the opening factor of the flow control valve. This effect can be seen comparing the left plots with the right ones.

There is a big difference between of a first half and the second half of a cycle. The output massflow has a big peak and is nearly completed in the first half and a small flow in the second half. The input massflow has its maximum also in the first half and again a smaller increase in the second half. This is caused by an increasing volume of the actuator for increasing stroke.
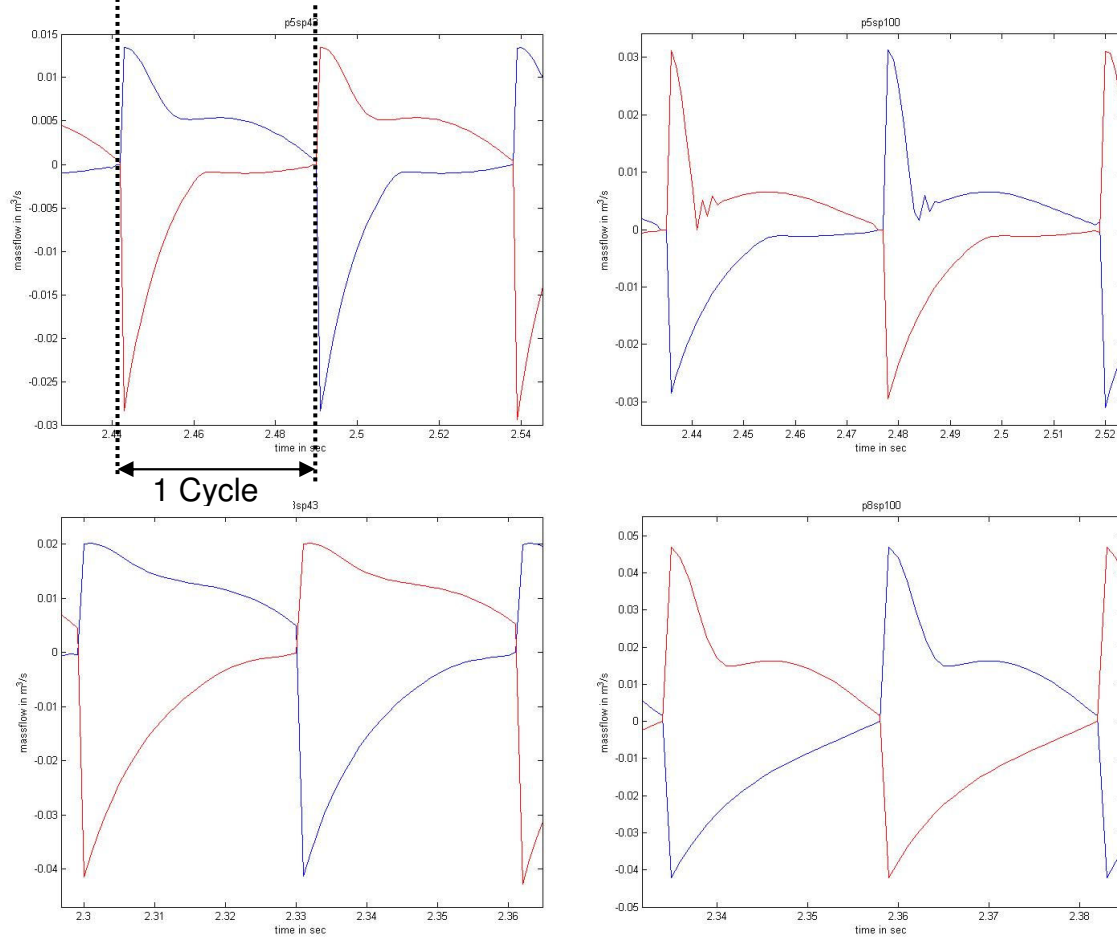
Figure 5-8 Massflow for different supply pressures and different opening factors

5.4.2   Pressure

As expected is the evolution of the pressure for a lower supply pressure slower which causes a smoother switching characteristic. The qualitative behaviour in the first and second half of cycle is similar to that of the massflow.
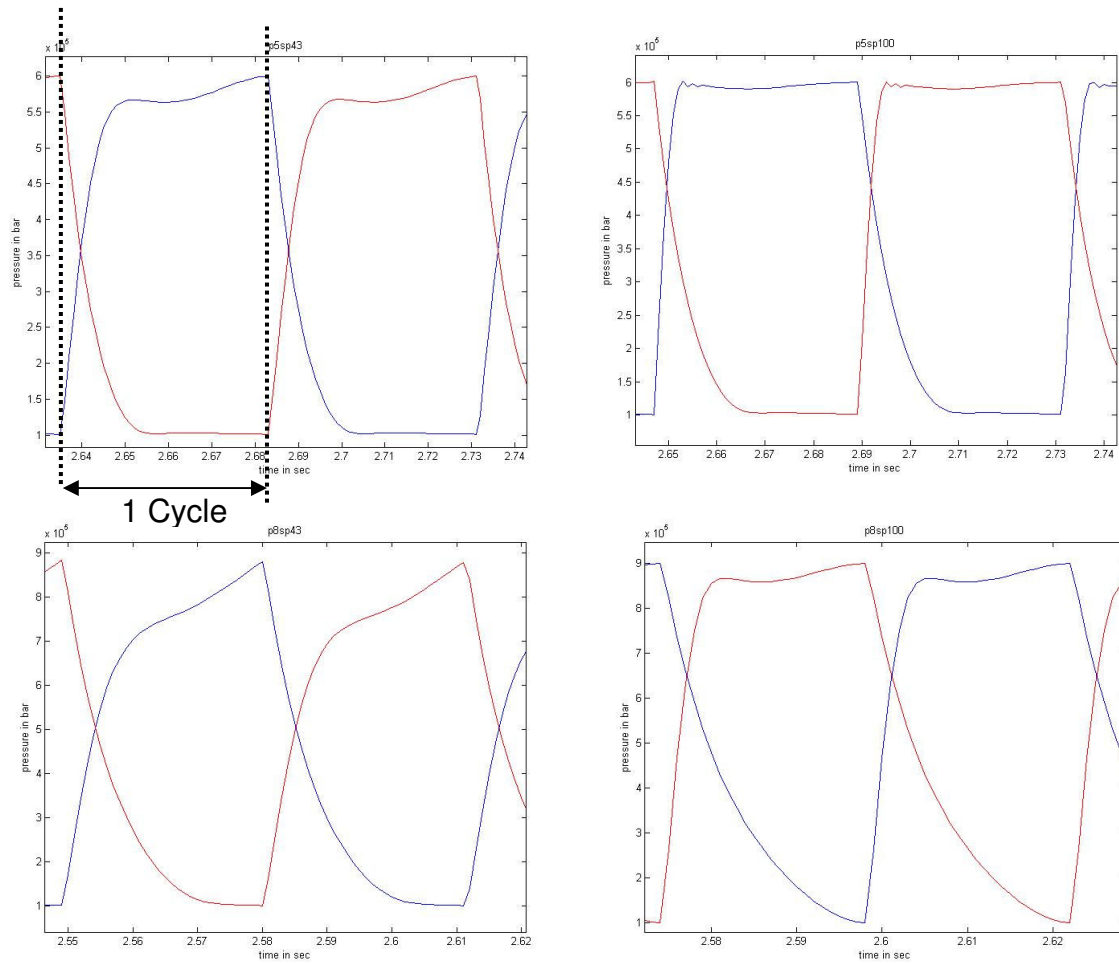

Figure 5-9 Pressure evolution for different supply pressures and different opening factors

5.4.3   Force

The evolution of the force generated by the actuators is depending on pressure and stroke. In the first half cycle it is a steep raise following the pressure. After the peak the force decreases with increasing stroke. After the switchpoint there is rapid decrease of the force. During a certain time interval after switching both muscles have a positive force and working against each other.
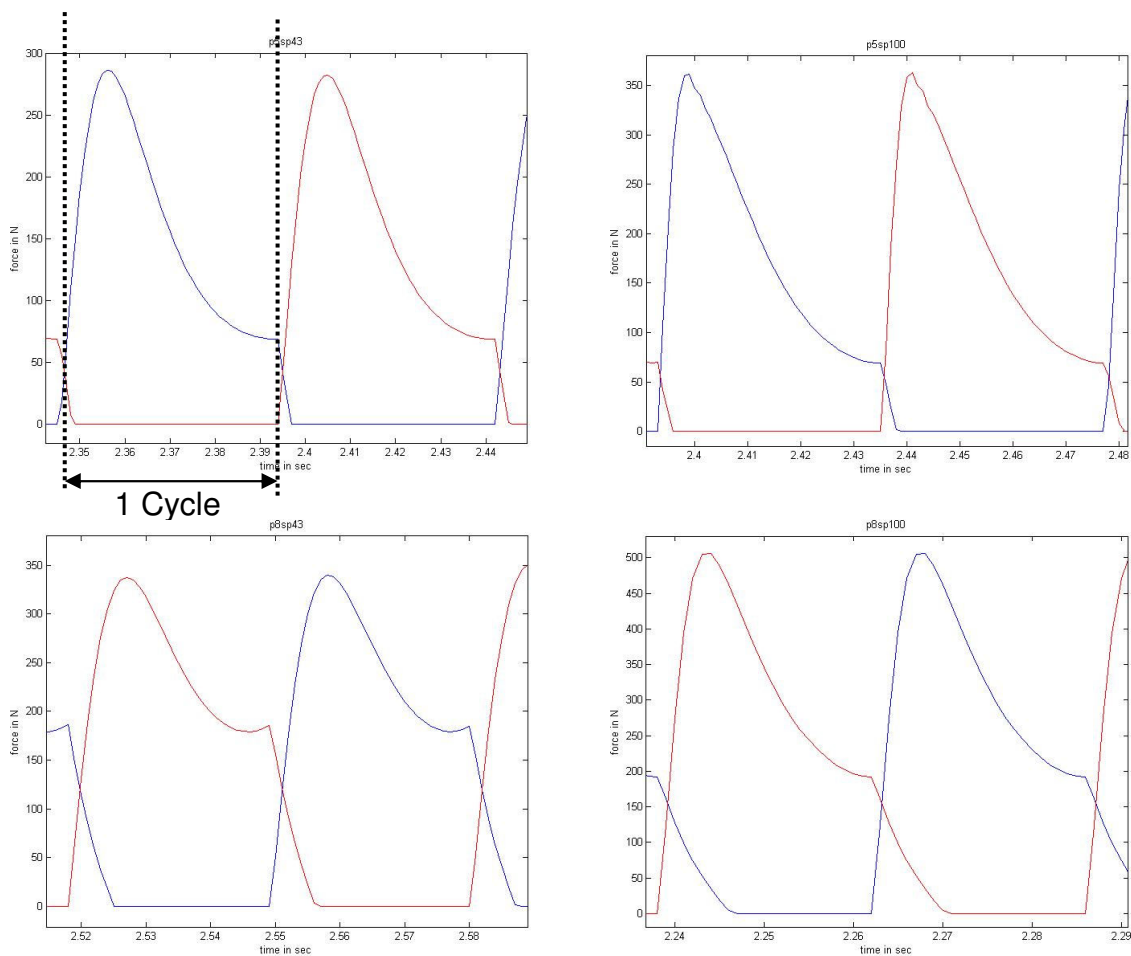

Figure 5-10 Force for different supply pressures and different opening factors

6 Conclusion

The goal of this work was to build an application of a Pneumatic Artificial Muscle which acts under high frequencies. A motor similar to a combustion engine was built up with two PAMs. The set-up was designed with a simple control unit. A row of measurements were run with the motor. The focus was the investigation of the angular velocity, especially of the acceleration phase and the steady state phase.

These measurements served as a base for the identification of a theoretical model of the motor. Several simulations validated the model of the motor.

In a future work a row of improvements is possible. For the real motor the control can be improved with an independent triggering of each muscle via two directional valves and a better measurement of the state of the crankshaft. Also a feedback of the actual angular velocity could be an expedient improvement.

Improvements for the simulation are a better implementation of the damping factor and a mathematic model for the flow control valve.

7 References

[1] Eberhard: Biomechanik, Institut für Technische und Numerische Mechanik, Universität Stuttgart

[2] Dillmann: Künstliche Muskeln als optimale Antriebe, Institut für technische Informatik, Universität Karlsruhe

[3] Festo AG & Co. KG: Esslingen

[4] Kerscher, Albiez, Berns: Joint Control of the Six-Legged Robot AirBug Driven by Fluidic Muscles, Universität Karlsruhe

[5] Daerden Frank: Conception and Realization of Pleated Pneumatic Artificial Muscles and their Use as Compliant Actuation Elements, Universität Brüssel

[6] Hildebrandt, Sawodny, Neumann, Hartmann: A Flatness Based Design for Tracking Control of Pneumatic Muscle Actuators, Seventh International Conference on Control, Automation, Robotics and Vision (ICARCV02) Dec2002, Singapore

[7] Manhartsgruber: Pneumatik (Ölhydraulik + Pneumatik II) PDF, März 2007

[8] http://en.wikipedia.org/wiki/Steady_state

[9] Baehr, Kabelac: Thermodynamik Grundlagen und technischen Anwendungen, Springer-Verlag Berlin Heidelberg, 2009

[10] Tondu, Lopez: ; Modelling and control of McKippen Artificial Muscle Robot Actuators, IEEE Control Systems Magazine, April 2000

[11] Chou, Hannaford: Measurement and Modelling of McKippen Pneumatic Artificial Muscles, IEEE Transactions on Robotics and Automation Vol. 12 No. 1, February 1995

[12] Neumann, Bretz, Volzer: Ein Positionierantrieb mit hoher Kraft: Positions- und Druckregelung eines künstlichen pneumatischen Muskels, Beitrag zum 4. Internationalen Fluidtechnischen Kolloquium, Dresden 25.-26.03.2004

[13] Verrelst, van Ham, Vanderborght, Lefeber, van Damme: Second generation pleated pneumatic artificial muscle and its robotic applications, Advanced Robotics Vol. 20 No. 7, 2006

[14] Aschenbeck, Kern, Bachmann, Quinn: Design of a Quadruped Robot Driven by Air Muscles, Biorobotics Laboratory, Case Western Reserve University Cleveland, Ohio

8 Appendix

The appendix is stored on the enclosed DVD and is organized as:

8.1 Report

8.2 Documents

- Print outs of references
- Additional publications related to the work

8.3 Matlab Files

8.3.1 Converting scripts

8.3.2 Experiments damping

8.3.3 Experiments motor

8.3.4 Simulation pressure valve

8.3.5 Simulation motor

8.4 Pictures_Videos

- Drawings
- Picture
- Films

8.5 Datasheets

8.6 Festo Programs